Journal of Structural Engineering & Applied Mechanics (2025) 8(4):279-311
DOI 10.31462/jseam.2025.04279311

RESEARCH ARTICLE

Shear performance of geopolymer concrete beams reinforced with industrial and waste fibers in the absence of stirrups

Barış Bayrak[1*]

[1] Kafkas University, Department of Civil Engineering, Kars, Türkiye

Article History

Received 25 September 2025
Accepted 29 November 2025

Keywords

Geopolymer concrete
Waste fibers
Beam
Shear behavior

Abstract

This research examines the feasibility of using waste fibers (yarn, fabric, hemp, plastic, iron powder, and iron shavings) as substitute shear reinforcements in slag-based geopolymer concrete (GPC) beams devoid of stirrups. It also compares their performance with that of beams reinforced with industrial fibers (steel, glass, and basalt). Beams measuring 50x150x750 mm were produced with 1% different waste and industrial fibers and subjected to three-point bending tests. The samples conducted were ten beams, which underwent three-point bending tests in relation to their load-deflection behavior, crack pattern, failure mode, strain distribution, energy dissipation, residual strength, and toughness. The findings show that industrial and waste fibers considerably improve the tensile strength of the GPC, preventing crack propagation and improving shear capacity. But performance is fiber type dependent. Among the waste fibers, hemp fibers made the highest contribution with respect to shear capacity, energy dissipation, and toughness compared to the other waste fibers and even to commercial fibers. On the contrary, iron powder had limited performance improvement, which was probably due to its low capability of bridging cracks. Among all the industrial fibers used, basalt and glass fibers exhibited the best compatibility with the GPC matrix, leading to the highest residual strength and toughness. Hemp and fabric are waste fibers; however offer the highest levels of energy dissipation owing to their pliability and high energy absorption. Moreover, the research indicates that the experimental shear capacity is also lower than the values predicted by international codes, including ACI318-19, Eurocode-2, and the fib Model Code 2020. These codes were found to be underestimating the shear strength of GPC beams, indicating a need for customized proposals. Thus, the research highlights the possibility of waste fibers as being sustainable and cost-effective for the reinforcement of geopolymer concrete.

1. Introduction

Humanity has aimed to build and improve sustainably since the beginning of the twenty-first century. The continuous increase in the global population is leading to a heightened demand for infrastructure each day. This results in to increase in the demand for cement production, which is widely used in structures [1-4]. On the other hand, reinforced concrete is the most important material for the construction industry because of

* Corresponding author (bbayrak@kafkas.edu.tr)
eISSN 2630-5763

its high strength and versatility. It is commonly used for beams, slabs, columns, and foundations in buildings and infrastructure projects. However, the use of traditional Portland cement-based concrete in construction has raised concerns about its negative environmental impact due to its high carbon footprint. In recent years, as a result of its lower environmental footprint, superior durability, and greater strength, geopolymer concrete has become a noteworthy alternative to conventional Portland cement-based concrete. The term geopolymer was first defined by Professor Davidovits in 1979, referring to a broad spectrum of binders that consist of a network of molecules interconnected by covalent bonds [5, 6]. Geopolymer concrete is made from industrial waste materials such as fly ash, slag, and rice husk ash [7-9]. These materials are mixed with an alkaline solution, which triggers a chemical reaction that creates a binder that solidifies and hardens like traditional cement. There are various advantages associated with geopolymer concrete over Portland cement-based concrete, including a lower carbon footprint, higher compressive strength, and greater resistance to corrosion and fire [10-12]. On the other hand, a polymerization process is responsible for the chemical reaction. In geopolymer concrete, this polymerization reaction unfolds rapidly, involving a chemical interaction between the minerals silica and alumina that results in the formation of a three-dimensional polymeric chain or tetrahedral network [13].

However, geopolymer concrete has some drawbacks, including its brittle behavior and low tensile strength. The tensile strength to compressive strength ratio of geopolymer concrete is too low that be comparable to conventional concrete [1]. To overcome these limitations, researchers have been investigating the use of various kinds of fibers, including natural fibers, synthetic fibers, and hybrid fibers, to reinforce geopolymer concrete. Fiber reinforcement can improve the mechanical properties of geopolymer concrete by enhancing its tensile and flexural strength, ductility, and toughness [5, 14, 15]. Moreover, the advantage of fiber is to improve the post-elastic properties and energy dissipation capacity of concrete after fractures. Another advantage of using fiber in the geopolymer concrete mixture is to prevent crack formation [16]. Among the different types of fibers, hybrid fibers are particularly promising because they combine the advantages of various kinds of fibers, such as the high strength and stiffness of steel fibers and the high aspect ratio and durability of polypropylene fibers. Hybrid fibers can also improve the resistance of geopolymer concrete to various types of loading, including flexural and shear forces. The performance of the fibers is influenced by several properties, such as the volume of the fiber, its geometry, orientation, type, and the attributes of the fiber matrix present in the mixture [16, 17]. Using a single type of fiber in a mixture improves the mechanical and ductility properties of geopolymer concrete. However, this improvement has a limited range. So, using hybrid fiber in geopolymer concrete, which is reinforced with two or more different types of relevant fiber, improves more properties to compare the geopolymer concrete with a single type of fiber. But choosing the relevant fibers is too important to achieve the synergistic effect. Cracks in concrete can develop at multiple stages and in varying sizes, thus employing fibers of different lengths presents a viable solution to this challenge. A well-engineered composite system facilitates beneficial interactions among the fibers, ultimately yielding superior performance in the hybrid system relative to a monofiber composite. The fundamental aim of utilizing a combination of diverse fiber types is to mitigate cracking in various areas of the cementitious material, addressing differences in size and occurring at different loading phases [18-20].

Recycled concrete composed of waste fiber represents a sustainable building material that effectively utilizes both waste fiber and construction debris. This innovative approach not only encourages the adoption of recycled concrete but also plays a crucial role in environmental conservation. The addition of waste fibers can increase the properties of the concrete matrix, reducing the likelihood of cracking and failure under shear force. This is because the fibers act as reinforcement, distributing the load more evenly throughout the concrete [21, 22]. Waste fibers can also enhance the durability of the concrete by improving its resistance to abrasion, impact, and weathering. This is because the fibers act as a barrier to prevent the ingress of moisture, salt, and other harmful substances that can cause corrosion and degradation. Furthermore, the use of waste fibers in reinforced concrete (RC) beams under shear force can provide a sustainable solution by reducing the amount of waste material that goes to landfills. This approach can aid in preserving natural resources and minimizing the carbon footprint associated with the construction sector [23, 24]. Waste fibers are often cheaper than traditional reinforcement materials such as steel, making them a cost-effective solution for RC beams under shear force.

Previous research indicates that the shear strength of geopolymer concrete (GPC) beams is similar to that of traditional reinforced concrete (RC) beams. However, the narrow ranges of waste materials are used as fibers in GPC beams under shear force, and relatively without the stirrup limit design applicability of GPC beams in practice. Most of the existing studies focused on steel [25], glass [26], basalt [27], or polypropylene fiber [28], etc., but research on waste fibers in relation to structural elements, design, and application remains limited. In particular, studies examining the shear behavior of geopolymer concrete (GPC) are scarce when juxtaposed with those involving ordinary Portland cement concrete.

Over the last several decades, a significant number of studies have been performed to evaluate the shear performance of GPC beams under shear loads, especially those that do not employ stirrups or incorporate waste materials into the mix. Aldemir et al. [29] performed a bending test to determine the shear behavior of RC beams made from construction and demolition waste-based geopolymer concrete. An investigation was conducted to assess the impact of shear-span ratio on the shear performance of several concrete variants, including geopolymer concrete with recycled aggregates, geopolymer concrete with natural aggregates, and both recycled and natural aggregate concrete. The results of the testing demonstrated that specimens with an a/d ratio of 1.65 exhibited a combined shear-flexural failure, which was dependent on the application of recycled aggregate. The research conducted by Wu et al. [30] involved shear testing on 21 reinforced concrete beams, aiming to explore the impact of several parameters, including the type of concrete, its strength, the ratio of longitudinal reinforcement, the strength of the longitudinal bars, the shear span-to-depth ratio, and the overall depth of the beams. In their study, Madheswaran et al. [31] analyzed the effects of shear span-to-depth ratios of 1.9 and 2.5, along with transverse bar ratios of 0, 0.56, 0.74, and 1.12%, on the shear strength of eight reinforced T-beams composed of fly ash-based glass composites, which had compressive strengths ranging from 30 to 44 MPa. The study by Visintin et al. [32] details the outcomes of eight beam tests on reinforced geopolymer concrete that did not incorporate stirrups, as well as the results from four direct shear tests conducted under conditions of low confinement. Significantly, the direct shear test results demonstrate that the shear friction properties of the geopolymer concrete utilized in this experimental study are consistent with those of established ordinary Portland cement (OPC) concrete. Maranan et al. [33] found that the beam with spiral reinforcement exhibited shear strength and deflection capabilities that surpassed those of the conventionally reinforced beam by 20% and 120%, respectively. Abdullah et al. [34] performed experiments to examine how the type of concrete and the shear span influence the shear strength of Ordinary Portland Cement (OPC) beams and Geopolymer Concrete (GPC) beams. The research conducted by Hussein et al. [35] involved a numerical examination of the shear performance of geopolymer concrete beams lacking stirrups, employing the ANSYS software to analyze the effects of various fiber reinforcements, including steel, synthetic polypropylene, polyvinyl alcohol, and carbon fibers. The outcomes indicated that the use of steel fibers resulted in a higher load failure threshold for the specimens, while the integration of carbon fibers notably enhanced the ductility of the beams.

The rising interest in the application of waste fibers within geopolymer concrete highlights the necessity for more extensive research to gain a thorough understanding of their impact on the behavior of reinforced concrete (RC) beams. Notably, there is a demand for further studies to evaluate how various waste fiber types influence the mechanical properties of geopolymer concrete. Therefore, this research seeks to investigate the role of waste fibers in the shear behavior of RC beams made from geopolymer concrete.

Chen et al. [36] propose a novel assembled reinforcement cage (ASC) system that segments traditional stirrups to address the reinforcement integration problem in 3D concrete printing. One of the key findings of the study is that 3D-printed beams without stirrups exhibit significantly lower cracking and bearing capacity. Zhu et al. [37] experimentally and numerically investigate the shear capacity variability in stirrup-free RC beams. They show that shear failure in stirrup-free beams is highly variable, with differences of up to 65% between specimens. Jia et al. [38] investigated the size effect on the dynamic shear behavior of RC beams under low-velocity impact. The analyses show that the size effect is much more pronounced in stirrup-free beams, with normalized displacement increases reaching up to 211%. This is due to the faster crack expansion and shear deformation progression in stirrup-free beams. This study by Lin et al. [39] investigated the effect of high-performance composite macrofibers (HPCF) on the shear capacity of beams without stirrups (without form reinforcement). Experiments show that even the addition of a small amount of HPCF significantly increases the shear strength of beams without stirrups. Rasheed et al. [40] developed regression models using a large database to predict the shear capacity of FRP-reinforced concrete beams without stirrups. They emphasized that shear prediction in beams without stirrups is difficult due to the low modulus of elasticity and brittle behavior of FRP. Resende et al. [41] investigated the shear behavior of GFRP-reinforced concrete beams, particularly in the case of stirrups, through critical crack kinematics. Experimental studies showed that wider oblique cracks form in GFRP beams without stirrups due to the lower modulus of elasticity and a reduced contribution of aggregate interlocking.

In this study, a total of one reinforced slag-based GC (RSGC) beam with a stirrup as a reference and nine RSGC beams without a stirrup were manufactured to investigate the effect of waste fibers. Three RSGC beams without stirrup were produced from geopolymer concrete with steel, basalt, and glass fibers preferred by researchers in the literature. Six beams were produced by using waste materials as fibers in the geopolymer mixture. Yarn, fabric, hemp, plastic, iron powder, and iron shavings were used as waste fibers. Waste yarn and waste fabric are polyester-based waste materials obtained from sewing workshops in the textile industry. Waste plastic is a recycling material used for the production of plastic materials. Iron powder and iron shavings were obtained from the lathe workshops. Hemp waste was obtained after this material was used in the agricultural industry. It was aimed to investigate the effect of using waste materials as fibers on the shear performance of RSGC beams. Therefore, RSGC beams with fibers were produced without shear reinforcement.

For the reasons emphasized above, this study aims to experimentally investigate the effect of using waste materials (yarn, fabric, plastic, iron powder, iron shavings, and hemp) as fibers on the shear performance of RSGC beams without stirrup. In addition, steel, glass, and basalt fiber RSGC beams without stirrup were produced, and the waste fibers were compared with these fiber types. It is also aimed to contribute to waste management by using waste fibers in sustainable and environmentally friendly geopolymer concrete. The shear properties of RSGC beams such as shear capacity, load-displacement curve, failure mode, residual strength, toughness, toughness index, energy dissipation capacity and comparison of recommended codes (ACI318-19, Eurocode-2, Italian code DM 204, fib Model Code 2020 approach, Swiss code SIA 262, Canadian standard CSA A23.3.04, Japanese standard JSCE, British standard BS8110–1, and Australian standard AS 3600) for shear strength of beams without stirrup were evaluated to establish the effect of waste fiber in geopolymer mixture. The shear behavior of RSGC beams manufactured by using waste fiber in geopolymer concrete is limited in the literature. The study reported in this paper aimed to make a significant contribution to this field to understand the behavior of RSGC beams with waste fiber under shear force.

2. Materials and experimental program

In this study, an experimental investigation was conducted on 10 geopolymer concrete beams subjected to monotonic loading conditions, specifically focusing on shear. The following sections will provide a comprehensive discussion of the materials, the configuration of the test setup, the instrumentation utilized, and the results obtained from the material testing.

2.1. Materials properties

The production of geopolymer concrete involves the utilization of ground granulated blast furnace slag (GGBS), in compliance with the ASTM C989 [42] standard. GGBS was supplied from the OYAK cement factory in Zonguldak province. GGBS is characterized by a high content of amorphous phase. The chemical composition of GGBS is detailed in Table 1. The specific gravity and specific surface area of GGBS are measured at 2.89 g/cm³ and 5520, respectively. Furthermore, silica fume (SF) was incorporated as a binder in the Geopolymer Concrete (GPC) mixture, with a specific gravity of 2.24 g/cm³. SF contains more than 90% silica (SiO_2), which contributes to its status as the binder with the most substantial specific surface area among various binders. The chemical composition of SF is detailed in Table 1. The X-ray diffraction (XRD) patterns of GGBS and SF are shown in Fig. 1. Furthermore, Fig. 2 presents the results of the particle size analysis. The GPC mix incorporated two varieties of aggregates, specifically coarse and fine aggregates, to improve the overall concrete composition. Fine aggregates are characterized by particle sizes of 0 to 4 mm, in contrast to coarse aggregates, which range from 4 to 16 mm. The aggregates possess a specific gravity of 2.65 g/cm³. Coarse and fine aggregates were supplied from Balsoy Beton company in Erzurum province. In the formulation of the GPC mixture, quartz aggregates with diameters ranging from 1 to 3 mm were incorporated as coarse aggregate. Quartz aggregates were supplied from the quarry in Denizli province. The specific gravity of these quartz aggregates is 2.65 g/cm³, and they contain 53.2% silicon dioxide (SiO2) by weight. In this research, three varieties of aggregates were utilized: quartz aggregate, coarse aggregate, and fine aggregate, with their respective gradation curves depicted in Fig. 2. In the geopolymer mixture, quartz aggregate was incorporated primarily as an inert filler material to improve hardness, dimensional stability, and matrix–aggregate bonding. Additionally, locally sourced natural aggregates were included to ensure proper gradation and workability, providing a homogeneous and dense structure in the slag-based geopolymer concrete. The alkali activators employed in the geopolymer slurries included sodium hydroxide (NaOH) and sodium silicate (Na_2SiO_3). A 12 M solution of NaOH was prepared at a controlled temperature of 20 °C, 24 hours in advance of the casting. To achieve the desired workability, the sodium silicate-to-sodium hydroxide (Na2SiO3/NaOH) ratio was determined to be 2.5, in alignment with previous research findings [43, 44]. The determination of the mix proportions was based on findings from previous studies [45-47], aiming to achieve the targeted workability and compressive strength. Table 2 provides an overview of the proportions for the three GPC mixtures.

Table 1. Chemical composition of GGBS, SF, and quartz

%	CaO	SiO_2	Al_2O_3	Fe_2O_3	MgO	Na_2O	K_2O	SO_3	LOI
GGBS	36.4	33.1	19.9	0.5	8.8	0.2	0.4	0.5	0.2
SF	0.3	95.6	0.2	0.2	0.2	0.1	0.2	0.3	2.1
Quartz	53.2	0.4	0.1	0.1	0.4	0.2	0.1	0.1	-

Table 2. Proportions (kg/m^3) of geopolymer mix

GGBS	SF	Quartz	Coarse aggregate	Fine aggregate	Sodium silicate	Sodium silicate
750	100	250	250	250	425	170

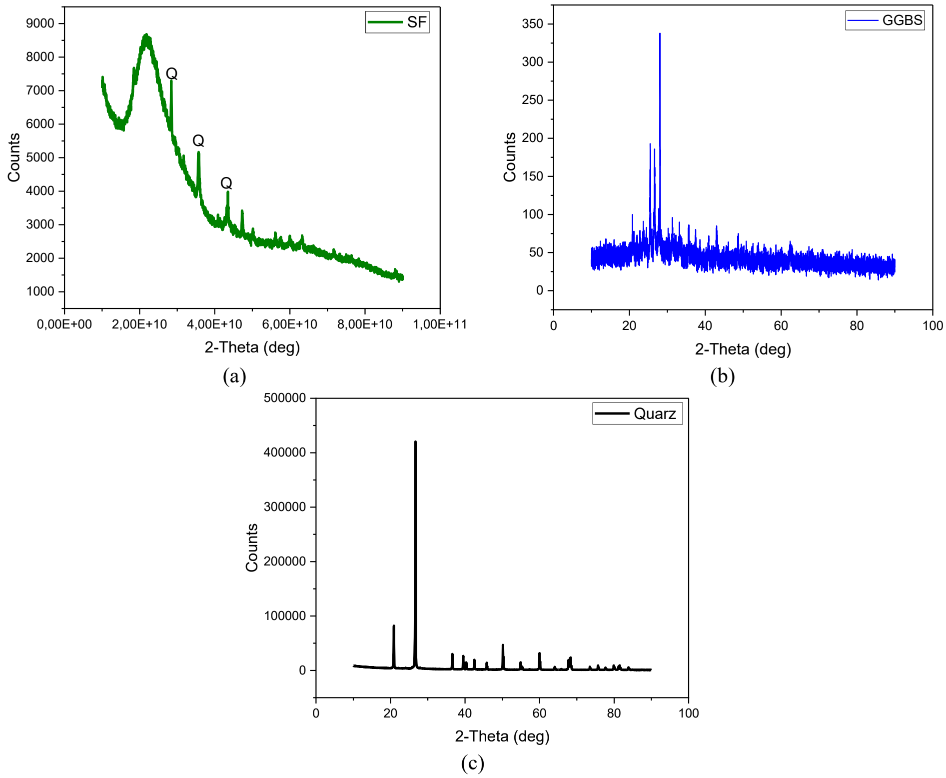

Fig. 1. XRD pattern of (a) GGBS, (b) SF, (c) quartz

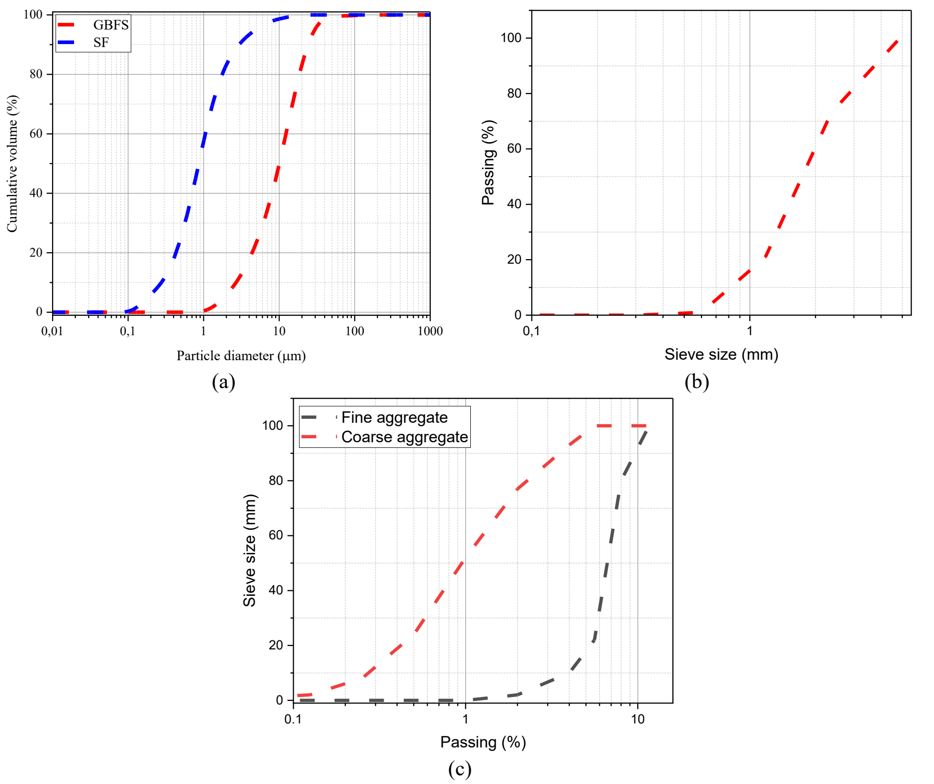

Fig. 2. Particle size analysis (a) GGBS and SF, (b) quartz aggregate, (c) fine and coarse aggregates

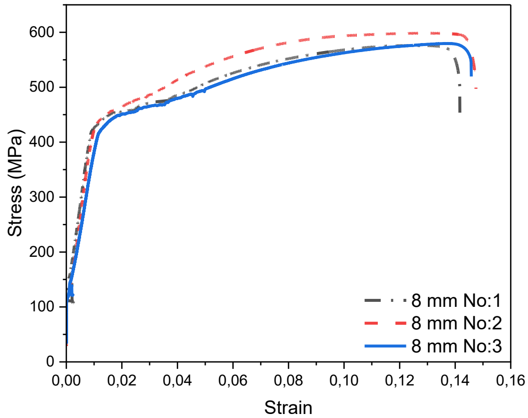

Fig. 3. Stress-strain curves of 8 mm rebar

Table 3. Technical properties of steel, glass, and basalt fibers

Property	AR-glass fiber	Basalt fiber	Hooked steel fiber
Diameter (mm)	0.40	0.43	0.5
Length (mm)	25	30	30
Tensile strength (MPa)	3200	4500	2000
Density (g/cm3)	2.60	2.80	7.81
Young's modulus (GPa)	73	90	200
Appearance			

Table 4. Characteristics of the waste fibers (Average ± standard deviation)

Material	Diameter/cross section (mm)/(mm.mm)	Length (mm)	Tensile strength (MPa)	Young's modulus (MPa)	Density (g/cm^3)
Waste plastic	4∓1	-	25-40	1-2	0.9
Hemp fiber	10∓2×2∓0.5	30∓18	550-900	70	1.2
Waste iron powder	0.2∓0.1	-	1100	205	7.80
Waste iron shavings	11∓2×2.3∓0.5	28∓15	1100	205	7.80
Waste polyester-based yarn	0.15∓0,05	31∓17	4.5-7.5	-	1.36
Fabric materials	40∓2.5×1∓0.3	29∓18	4.5-7.5	-	1.36

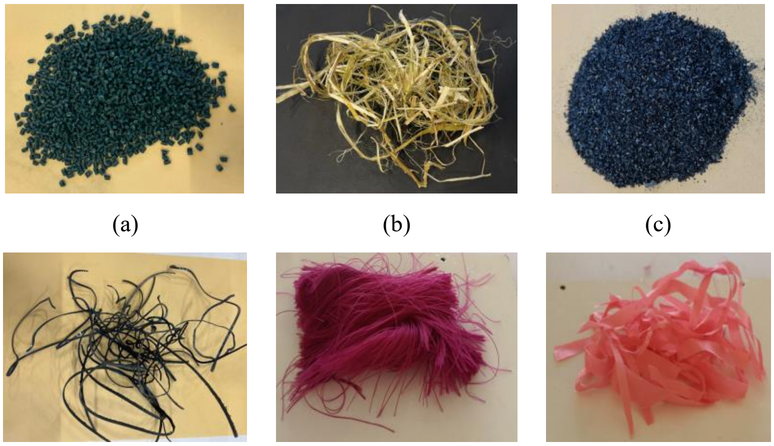

Fig. 4. Waste fibers used in the study: (a) plastic, (b) hemp, (c) iron powder, (d) iron shaving, (e) yarn, and (f) fabric

The strain-stress curve for the 8 mm rebar, employed for both longitudinal and transverse reinforcements in the reference specimen, is presented in Fig. 3. According to the manufacturer's specifications, the average yield strength, tensile strength, and elongation at break of the rebar, derived from three samples, are recorded as 455 MPa, 584 MPa, and 13.21%, respectively. Moreover, the maximum average ε of three samples is 0.145.

Nine different fibers were used in the geopolymer concrete mixture. Three of these fibers are the most preferred by researchers in the literature: hooked steel fiber, AR-glass fiber, and basalt fiber. The technical properties of steel, glass, and basalt fibers are presented in Table 3. The beams were cured for 7 days at 23 ± 2°C and 40 ± 5% relative humidity until the test day.

Six waste fibers were used in the geopolymer mixture. Photographs of waste fibers are shown in Fig. 4. The fibers, as illustrated in Fig. 4, were randomly clustered and exhibited a range of geometrical characteristics. Furthermore, the majority of the fibers were not aligned straight like those found in commercial products such as steel, glass, or basalt fibers. To evaluate the geometrical characteristics, a random sample of 1000 g of waste fibers was chosen, and the dimensions of each fiber were recorded. Since some fibers were circular in shape (such as waste plastic and waste iron powder), their diameters were measured. Since some fibers (such as hemp fiber, iron shaving, waste polyester-based yarn, and fabric materials) were rectangular in shape, their cross-sectional area and length were measured. Due to their considerably longer length relative to commercially available fibers, the waste fibers could not be employed in the production of traditional fiber-reinforced concrete. However, they proved to be appropriate for geopolymer concrete production, provided they underwent further processing, including reduction to smaller lengths. The rectangular waste fibers were cut into lengths of 12 to 30 mm to ensure compatibility with industrial fibers (glass, steel, and basalt).

The geometry and mechanical properties of waste fibers are shown in Table 4. First, waste plastic fibers were used. Waste plastics were obtained from waste materials used in the production of plastic materials. The geometry of waste plastics is not a perfect circle, but is very close to a circular form. In addition, since the surfaces of plastic particles are rough, it can increase the adhesion between the concrete matrix and the plastic particle. The diameter of waste plastic particles is 4∓1 mm. Second, it is the waste form of the hemp plant used in the agricultural industry. Hemp fiber is the waste part of this plant after it is processed in the agricultural industry. Hemp fiber is rectangular in shape, and its tensile strength is in the range of 550-900. Third and fourth, waste iron powder and iron shavings. Waste iron powder and iron shavings were obtained as waste from lathe workshops. Fifth and sixth, waste polyester-based yarn and fabric materials were used as fibers. These fibers were also obtained as waste from the textile industry. 1% fiber was used in all fiber blends. Although some of the selected waste materials, such as waste plastic and iron powder, are granular rather than fibrous in geometry, they were intentionally included as fiber-type reinforcements. These materials exhibited surface roughness and stiffness that enabled effective stress transfer and microcrack bridging within the geopolymer matrix. Therefore, they were functionally treated as discontinuous fiber-like inclusions contributing to toughness and post-cracking behavior.

The preparation of all GPC mixture batches was conducted using a concrete mixer of the rotating drum type, which has a capacity of 100 liters. The mixing operation was carried out in a two-step process. The first step involved the pre-mixing of solid materials, including GGBS, SF, quartz aggregate, fine aggregate, and coarse aggregate, for a period of five minutes. In the second step, the alkali activators, sodium silicate and sodium hydroxide, were incorporated, followed by an additional three minutes of mixing. For GPC blends that contained fibers, these fibers were added after the alkali activators. This systematic approach was consistently applied to all specimens, with the mixing duration set at five minutes to ensure the desired consistency and adequate mixing of the components. The assessment of the geopolymer mortar's workability was conducted in compliance with ASTM C1437-15 [48].

The average flow diameter of the GPC mixture without fiber was 250∓20 mm. Adding steel fiber, waste plastic, waste iron powder, and waste iron shaving to the GPC mixture did not significantly affect the flow diameter. The average flow diameter of the GPC mixture with these fibers was between 210 mm and 230 mm. On the other hand, the average flow diameter of the GPC mixture with yarn was 170∓20 mm. The addition of waste fabric, hemp fiber, basalt fiber, and glass fiber to the GPC mixture significantly reduced the workability. The flow diameter of these fibrous GPC mixtures varied between 110 mm and 150 mm, and vibration was applied while pouring these mixtures into the molds. The three cylinders, all with dimensions of 100×200 mm, were fabricated from the identical batch utilized for the GPC beams. After the casting was completed, all beams and cylindrical specimens were shielded with plastic sheets and cured in a controlled laboratory environment until the testing dates. Three cylindrical specimens were utilized to evaluate the compressive strength of the GPC mixtures. All specimens were demolded within 24 hours and allowed to air cure for seven days under laboratory conditions. Literature sources [49-52] suggest that the chemical reactions occurring in geopolymer are characterized by a rapid polymerization process, enabling these materials to achieve substantial strength during the initial curing phases. As a result, the goal was to harness the advantages of early high strength associated with geopolymer.

2.2. Details on test specimens

In this investigation, the shear performance of GPC was evaluated in scenarios both with and without fiber reinforcement. A reference beam with stirrups was selected, along with nine stirrup-free beams, to examine different potential failure mechanisms. The geometric properties and reinforcement configurations of the tested specimens were established in compliance with ACI318-19 [53]. The specimen details of one RSGC beam with a stirrup and nine RSGC beams without a stirrup are shown in Fig. 5. The dimensions of the beam were as follows: a width of 150 mm, a height of 150 mm, and a length of 750 mm, with a shear span measuring 350 mm. The effective depth (d) of the beams was 120 mm, resulting in a shear span-to-depth ratio (a/d) of 2.92. The shear span-to-effective depth ratio (a/d = 2.92) was selected following previous studies and design recommendations (ACI 318-19) to ensure a shear-dominated response. This ratio facilitates the formation of diagonal shear cracks before flexural yielding, allowing a clearer assessment of the fiber contribution to shear capacity.

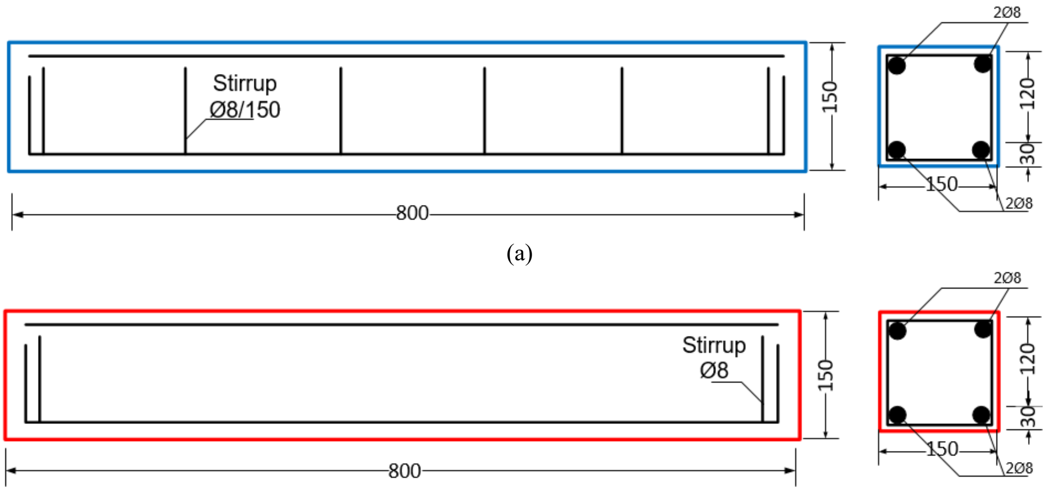

Fig. 5. Reinforcement details of the test specimens (a) with stirrup, (b) without stirrup (all dimensions are given in mm)

Table 5. Test parameters

Specimen	ρ_l	ρ_t	Fiber type	Fiber ratio	fc (MPa)
B-R	0.0056	0,0086	-	0%	32.23
B-S	0.0056	-	Hook steel	1%	42.20
B-B	0.0056	-	Basalt	1%	50.61
B-G	0.0056	-	AR-glass	1%	48.25
B-WP	0.0056	-	Waste plastic	1%	42.40
B-HF	0.0056	-	Hemp fiber	1%	27.50
B-IP	0.0056	-	Waste iron powder	1%	51.22
B-IS	0.0056	-	Waste iron shavings	1%	54.92
B-Y	0.0056	-	Waste polyester-based yarn	1%	40.83
B-FM	0.0056	-	Fabric materials	1%	44.11

Standard hooks at a 90° angle were employed at both ends of the beam to secure the longitudinal reinforcement bars. In accordance with the ACI318-19 [53], the reference beams met the minimum stipulation for stirrup spacing to prevent shear failure. All beams received reinforcement at both the top and bottom with two 8-mm diameter rebars (A_f = 100.5 mm^2), leading to a reinforcement ratio of 0.56%. The RSGC beams, which featured stirrups, utilized 8 mm diameter rebar positioned at 150 mm intervals along their length. In addition, two stirrups of 8 mm diameter were installed at the supports of the beam without stirrups to facilitate the construction of rebar cages. A concrete cover of 30 mm was consistently applied to the transverse stirrups on every side of the beams. The test parameters of the specimens are given in Table 5. Regarding the specimen name, the first letter B indicates the beam. The second letter R and S, G, WP, etc., indicate reference and type of waste fiber, respectively.

2.3. Test setup and instrumentation

Fig. 6 illustrates the three-point test configuration utilized for the shear test. This configuration is widely recognized in the literature [29, 30, 54-56] as a standard method for assessing the shear performance of beams. The beam was designed as simply supported, with one vertical load applied to its upper face. The shear span for the test specimens was determined to be 350 mm. Monotonic loading was conducted using a hydraulic jack with a capacity of 1000 kN, and a load cell of the same capacity was used to monitor the applied loads during all tests. The loading procedure for the shear tests consisted of applying increments of approximately 2 kN per second until the ultimate resistance of the specimens was achieved. The test was conducted under load control at a rate of 2 kN/s until failure. To evaluate the deflection at the center of the beam, Linear Variable Differential Transformers (LVDTs) were utilized. The LVDT was located midpoint of the beam. Two strain gauges were attached to measure the strain of longitudinal reinforcement and the concrete surface. A strain gauge was attached to the mid-point of the bottom flexural bars because it is the point where maximum tensile deformation is expected. A strain gauge was attached to the concrete surface at the midpoint and down to the concrete cover because it is the point where maximum compressive deformation is expected.

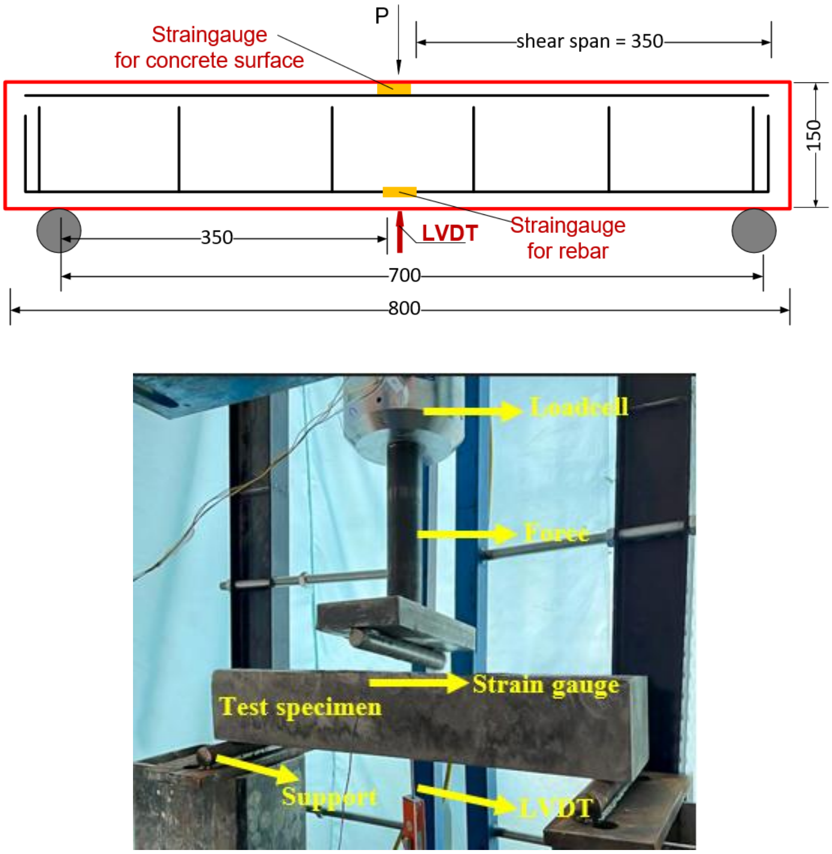

Fig. 6. Test setup (all dimensions are given in mm)

3. Test results

3.1. Load-midpoint deflection relationship

The load-midspan deflection relationship of tested beams is shown in Fig. 7. The relationship of load-deflection is comprises with the curves in literature studies [57-59]. The relationship of load-displacement of tested beams, apart from the normalized load-deflection graphs, is presented in Fig. 8. The forces that were monitored were normalized using the formula $P / \sqrt{f_c}bd$ to account for variations in compressive strength. Where P symbolizes the force (N), b and d symbolize the width and depth of the beam (mm), respectively, and f_c symbolizes the cylinder compressive strength of GPC (MPa). As shown in the figure, the specimens exhibit a load-deflection response that can be categorized into two separate phases. In the first phase, the graphs are linear until the first flexural fracture occurs, indicating the performance of the beams in an undamaged state. Following the emergence of the initial crack, the beams transitioned to a post-cracked behavior. During this phase, the load-deflection curves displayed nonlinear behavior, with a progressive decrease in stiffness observed until the peak load was attained. The linear increase was kept with the increase in load to the P_{cr} point. This interruption in the graph indicates a change in the relationship between load and displacement after the first crack appeared. This caused the rigidity of specimens to change due to the first crack. Therefore, the P_{cr}, P_y, $P_{max,}$ and P_u points were marked in the load-displacement graphs. It is seen that this trend indicates a significant reduction in performance immediately after reaching the maximum capacity. After the P_{max} point, as a result, the performance of the B-R specimen was adversely affected, highlighting the critical importance of ductility in the matrix phase for maintaining strength under stress. In the B-S specimen, the loss of strength after the maximum load exhibited better performance compared to the B-R specimen. This shows that the steel fibers provided good adhesion with the GPC matrix. The B-G and B-B specimens exhibited a similar pattern in their observations. Both the glass fiber and the basalt fiber provided good compatibility with the GPC matrix. In this case, there was no notable decline in the shear strength of the specimen after reaching the peak load. In B-Y, B-IS, and B-IP specimens, waste yarn, iron powder, and iron shavings have less effect on the sharp strength loss after the maximum load compared to other specimens. In these specimens, a more sudden strength loss was observed in the shear force due to shear cracks after reaching the maximum load, compared to other specimens.

The test results were summarized in Table 6. The table presents the critical load (P_{cr}) at which the first crack occurs in the specimens, along with the corresponding displacement value (Δ_{cr}). Following this, the load at yielding (P_y) and its associated displacement (Δy) are also included. Additionally, the maximum load (P_{max}) attained by each specimen, along with the displacement value at this peak load (Δmax), is detailed in the table. Given that various mixtures were utilized in the specimens, the concrete compressive strength varies among the specimens. Consequently, as the concrete compressive strength is not the focus of this study, a normalized load $P / \sqrt{f_c}bd$ was computed using the maximum load values listed in Table 6. Lastly, the ultimate load (P_u) and its corresponding displacement (Δu) are provided in the table, while the energy dissipation capacity (E) is derived from the total area beneath the load-deflection curve.

The maximum load (P_{max}) of the specimens changed significantly according to the type of fiber used in the GPC mixture. The minimum shear capacity was obtained with a value of 27.66 kN in the B-R reference specimen without a stirrup. In the absence of fibers in the GPC mixture, the tensile strength capacity of GPC remained limited. Thus, the shear force capacity remained limited when compared to the other specimens. Especially after the first crack occurred in the B-R specimen, the principal tensile stresses exerted on the beam led to a rapid decline in strength following the attainment of the maximum load. This phenomenon indicates a critical failure point where the concrete could no longer withstand the applied forces, highlighting the importance of incorporating appropriate reinforcement to enhance performance. The utilization of steel (SF), glass, and basalt fibers significantly influenced the shear force capacity, contributing to an enhancement in its overall performance. It has been reported [35, 57] that the utilization of SF in stirrup-free beams improved the shear force capacity. However, the utilization of iron-based waste shaving caused the P_{max} of the tested beam to increase significantly. The P_{max} of the B-IS beam using iron-based waste shaving was 62% higher than the reference specimen (B-R), but 8% lower compared to the B-S specimen using steel fiber. This result firstly showed that waste iron shavings can significantly increase the P_{max} in beams without stirrups. Secondly, it was concluded that it can also be used instead of hooked steel fiber. Especially, the surfaces of waste iron shavings have a very rough structure after lathe processing. This roughness caused a very effective adhesion between the GPC matrix and the fibers. Because of the effective adhesion between the fiber and the GPC, the defect rate around the waste iron shavings fibers decreased. Thus, the stresses occurring in these regions were effectively counteracted. Also, the P_{max} value of the waste B-IS specimen is 17% and 20% less than the P_{max} of the B-G and B-B specimens using glass and basalt fibers, respectively. These results also show that glass and basalt fiber performance can be achieved by optimizing the waste iron shavings fiber ratio. However, it was observed that the use of waste iron powder did not have a significant effect on the shear force. This type of waste fiber, especially in powder form, prevented it from having a bridging effect in preventing shear cracks. For this reason, the minimum shear force capacity in fiber beams was obtained in the B-IP specimen. Therefore, it is recommended by the author to use fine aggregate instead of fiber in the GPC or OPC mixture of waste iron powder in future studies.

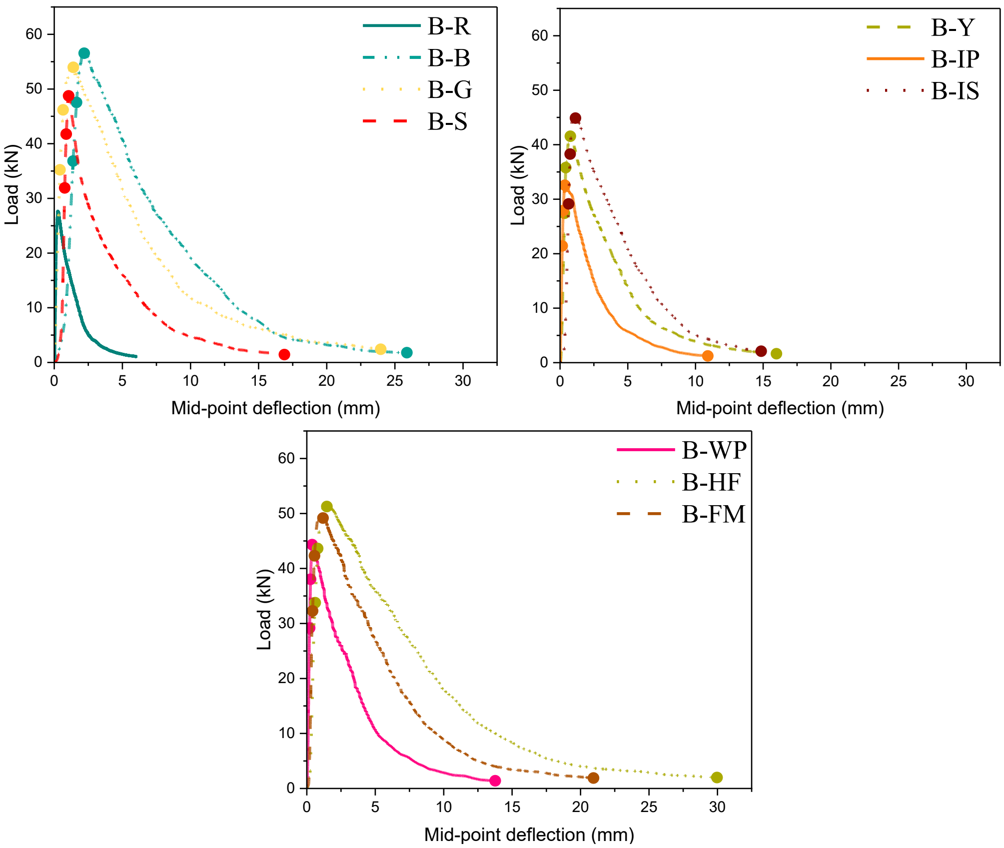

Fig. 7. Load-deflection curves

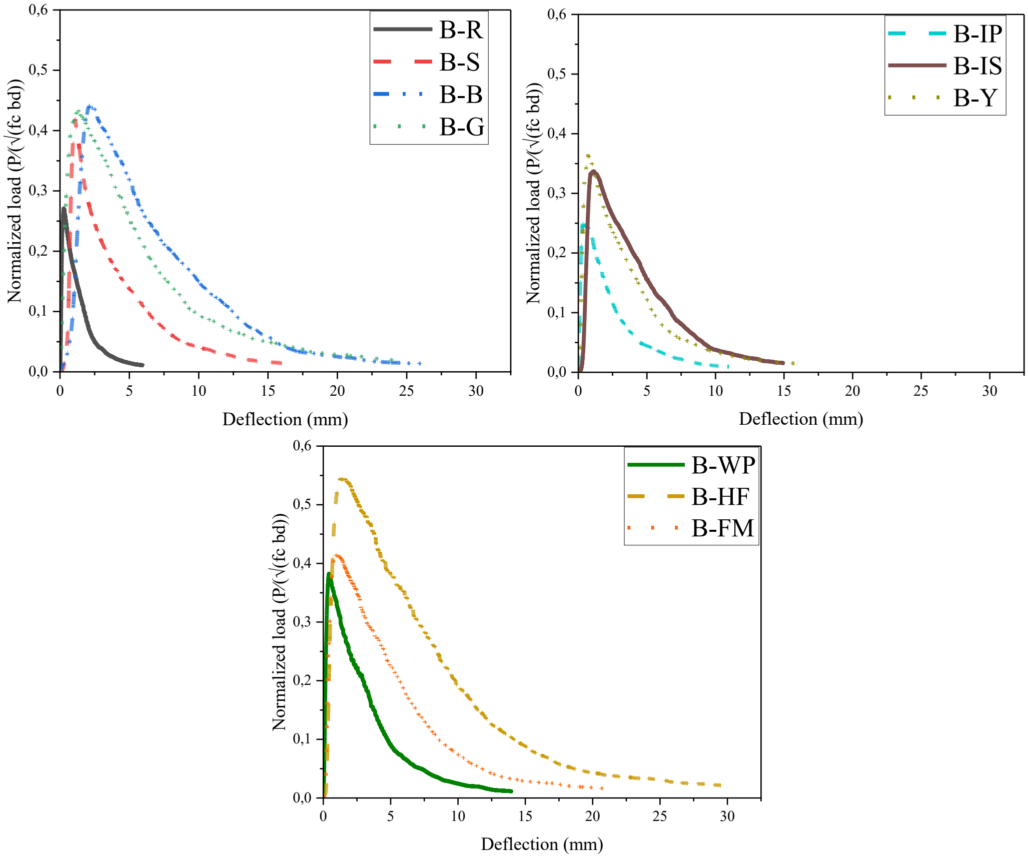

Fig. 8. Normalized load-deflection curves

Table 6. Summary of test results

Specimen ID	f_c (MPa)	P_{cr} (kN)	Δcr (mm)	P_y (kN)	Δy (mm)	P_{max} (kN)	$\frac{P_{max}}{\sqrt{f_c'}bd}$	Δmax (mm)	Pu (kN)	Δu (mm)	FM*
B-R	32.23	17.98	0.126	23.51	0.167	27.66	0.271	0.313	1.07	6.00	S
B-S	42.20	31.86	0.771	41.67	0.886	49.02	0.419	1.124	1.43	16.93	S
B-B	50.61	36.89	1.395	48.25	1.667	56.76	0.443	2.250	1.76	25.99	S
B-G	48.25	35.26	0.428	46.10	0.653	54.24	0.434	1.450	2.40	24.00	S
B-WP	42.40	29.13	0.204	38.10	0.278	44.82	0.382	0.394	1.32	13.97	F+S
B-HF	27.50	33.46	0.617	43.75	0.804	51.47	0.545	1.076	1.98	30.01	F+S
B-IP	51.22	21.35	0.163	27.91	0.247	32.84	0.255	0.342	1.22	10.98	F+S
B-IS	54.92	29.21	0.631	38.20	0.742	44.94	0.337	1.046	2.06	14.95	S
B-Y	40.83	27.35	0.332	35.76	0.428	42.07	0.366	0.864	1.63	16.00	S
B-FM	44.11	32.25	0.423	42.17	0.564	49.61	0.415	0.994	1.91	20.96	F+S

*FM: failure mode, S: shear, F: flexural, F+S: combined of shear and flexural

The use of waste plastic and yarn in the GPC mixture has a considerable influence on the P_{max}. Although the tensile strength capacity of these fibers is low, their effect on the P_{max} of the tested beam is critical. The reason for this situation is that waste plastics are waste and recycled materials, so their surfaces are quite rough. Surface roughness increased the adherence to the GPC matrix. In addition, since polyester-based yarn fibers have a significant elasticity capacity, this caused the shear force capacity to increase. The P_{max} of the B-WP and B-Y specimens using waste plastic and yarn fibers also exhibited a very effective performance compared to the specimens using industrial fibers (glass, basalt, and steel). In fact, the shear force capacity of the B-WS and B-Y specimens is 38% and 52% higher, respectively, compared to the reference specimen. These results also show that waste plastic and waste yarn have an effective performance as a transfer element in the beams. It is even mentioned that waste iron shavings have a significant effect on the shear force capacity. Since iron shavings are also an iron-based material, they can cause corrosion problems in beams that may be exposed to harsh environmental conditions. However, the absence of corrosion problems in waste plastic and waste yarn fibers provides advantages to these waste fiber types.

Among the waste fibers, the maximum shear force was reached in the B-HF specimen with a value of 51.47 kN. The striking point here is that although the 7-day compressive strength of the tested beam using hemp fiber is low (f_c = 27.5 MPa), the Pmax value is quite high. The reason for this situation is, firstly, that hemp fibers have quite high tensile strength (550-900 MPa). Secondly, hemp fibers have increased the resistance of the specimen against crack formation due to their high-energy absorption capacity. Hemp fibers also have high flexibility. Hemp fibers could not exhibit these advantages under axial pressure (for the determination of 7-day compressive strength). However, they exhibited the advantages of high-tensile strength, high-energy absorption capacity, and high flexibility in resisting shear forces. The principal tensile stresses originating from the shear force in the matrix were resisted by hemp fibers. Hemp fibers increased the weak tensile strength of the GPC matrix. Hemp fibers ensured that the stresses accumulated at weak points within the matrix were transferred to stronger areas. The shear force capacity of the B-HF specimen is higher than the steel fiber B-S specimen. In fact, when compared to basalt and glass fiber specimens, the shear force of the B-HF specimen is 9% and 5% lower, respectively. Despite this, it is seen that hemp fibers are a very ideal alternative for helping shear reinforcement. It is seen that the P_{max} of the waste fabric fiber specimen is also close to the hemp fiber specimen. Moreover, Sedan et al. [60] and Awwad et al. [61] also reported that hemp fiber leads to an improvement of the mechanical properties of concrete. It is seen that fabric fibers are effective in shear force capacity, especially due to their geometric structure. Since they have a rectangular cross-sectional area and a larger cross-sectional area compared to other fiber types, the effectiveness of fabric fibers is seen to be more visible.

3.2. Crack patterns and failure modes

The crack patterns and failure modes of test specimens are shown in Fig. 9. Observations indicated the presence of three failure modes: diagonal tension failure, shear compression failure, and flexural failure. Diagonal shear cracks generally formed in the beams. In addition, bending cracks were also observed together with diagonal shear cracks in some samples. As seen, the type of fiber used affected the crack width and failure mode. Shear and bending cracks were observed together in the B-WP, B-HF, B-IP, and B-FM specimens. In these specimens, the first crack occurred at the shear force load values of 29.13 kN, 39.46 kN, 21.35 kN, and 32.25 kN, respectively. It is seen that the P_{cr} value of the specimen, in which waste iron powder was used, is low. However, a relatively high P_{cr} value was reached in the beam where hemp fiber was used. In these specimens, the first crack occurred in the lower region of the beam midpoint (the outermost concrete section in the region under tensile stress) and suddenly. The length and crack width of the bending crack in the B-WP specimen are low compared to the other samples. Because of the low P_{cr} of the B-WP specimen, due to the low P_{max} and Δ_u values, the shear crack formed without increasing the crack width and number. Because of the limited deflection ability of the B-WP specimen (Δ_u = 13.97 mm), the shear crack formed immediately after the flexural crack, and the width of the shear crack increased with the increasing load. In the B-FM specimen, the flexural crack has a greater crack width and crack length compared to the B-WP specimen. This situation is caused by the fact that both the P_{cr} and Δ_u = 20.96 mm values of the B-FM specimen are higher than the B-WP specimen. The flexural crack observed in the B-IP specimen is also close to the B-WP specimen. Since the P_{cr} and Δ_u values of these two specimens are close to each other, the flexural crack distribution is also similar. However, the crack width of the flexural crack observed in the B-HF specimen is also limited.

It has been noted that the width of the diagonal shear crack in the B-HF specimen is reduced in comparison to the widths found in the other specimens. In addition, the number of shear cracks in the B-HF specimen is higher than in the other specimens. The elevated tensile stress and significant elasticity of hemp fibers contribute to an increase in the number of shear cracks as the applied shear force escalates. In the B-FM specimen, a relatively larger crack width was reached compared to the other specimens. In the specimens using waste plastic and basalt fibers, the diagonal crack width is limited. In the B-S specimen using steel fibers, the shear crack's width is more pronounced than that observed in the other specimens, particularly as a result of the steel fibers' bridging effect, which mitigates the propagation of cracks.

3.3. Strain of rebar and concrete surface

Compressive strains at the upper central face of the tested reinforced concrete beams were measured by considering the effects of different fiber types on the concrete surface. Simultaneously, the tensile strains in the primary reinforcement were evaluated by analyzing the impact of various fiber types on the strain present in the rebar. Compressive strain at the concrete surface and tensile strain at reinforcement of maximum load and ultimate load are shown in Tables 7 and 8. Maximum load-strain at maximum load curves are shown in Fig. 10. The analysis revealed a rise in the strains of compression and tension across all RSGC beams in relation to the reference beam. The results in Table 7 show that there are significant differences between the concrete strain values in the fibrous samples. The compressive strain values are higher in the B-IS specimen, especially when iron-based waste fibers are used, compared to the other samples. For example, the concrete strain values under ultimate load in the B-IS sample are approximately 244% higher than in the reference specimen (B-R). This situation shows that the specimen in which waste iron shavings are used provides effective compatibility with the GPC matrix, especially due to the rough surfaces of the shavings. The randomly distributed iron shavings in the GPC helped the concrete phase in resisting the compressive stresses. In addition, although the fibers caused more strain in the compressive zone in the B-G and B-B samples with mineral-based glass and basalt fibers, the samples in which organic-based yarn and iron powder were used had a limited effect on the compressive strain of the concrete surface compared to the other samples. It is observed that the waste yarn and iron powder are insufficient to resist the compressive stresses in the matrix in these specimens. The reason for this situation is that the distribution of these waste fiber types in the GPC matrix and the adhesion mechanisms are not sufficiently effective. In addition, it is seen that there is a relationship between the crack-preventing effect of the fibers and the compressive strain, depending on the bonding strength at the fiber-GPC matrix interface.

The fibers used in the GPC mixture have a significant effect on the strain in the reinforcement as well as on the concrete surface. Especially the use of basalt, glass, and steel fibers caused the stress value in the reinforcement to increase more than two times compared to the reference sample. Glass, basalt, and steel fibers were randomly distributed in the GPC matrix, preventing the formation of cracks around the reinforcement or causing them to form at a higher shear force value. Thus, the reinforcement was allowed to be stressed more. This shows that waste fibers are as effective on strain as industrial (glass, basalt, and steel) fibers. This situation shows that there is a strong bond between some waste fibers and the GPC matrix, and causes the strain values in both concrete and reinforcement to increase.

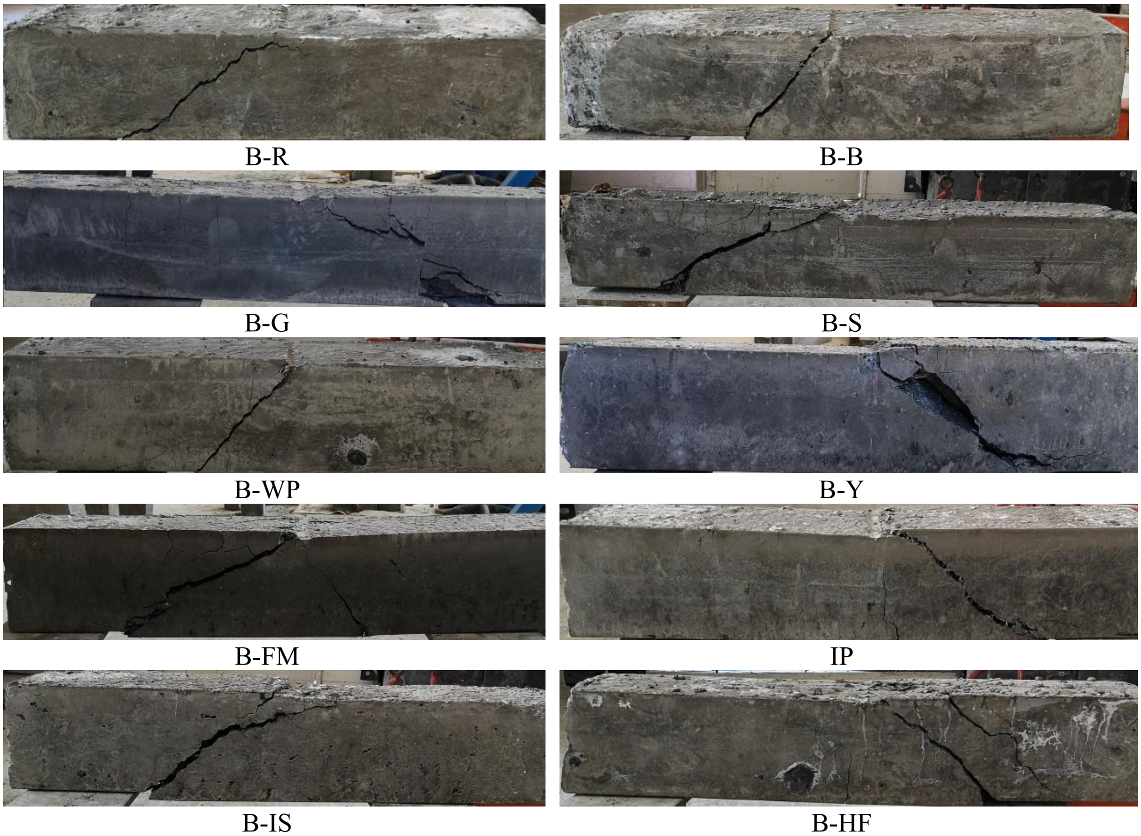

Fig. 9. Crack patterns and failure modes

Table 7. Compressive strain at the concrete surface

Specimen ID	f_c (MPa)	P_{max} (kN)	At maximum load		At ultimate load	
			Concrete strain (10-6) (mm/mm)	Decrease in strain (%)	Concrete strain (10-6) (mm/mm)	Decrease in strain (%)
B-R	32.23	27.66	591.8	-	854.7	-
B-S	42.20	49.02	793.1	34.0	1325.1	55.0
B-B	50.61	56.76	865.7	46.2	1631.7	90.9
B-G	48.25	54.24	875.8	48.0	1702.8	99.2
B-WP	42.40	44.82	794.0	34.1	1370.6	60.3
B-HF	27.50	51.47	866.8	46.4	1622.5	89.8
B-IP	51.22	32.84	631.6	6.7	1097.8	28.4
B-IS	54.92	44.94	998.7	68.7	2944.0	244.4
B-Y	40.83	42.07	876.2	48.0	1192.5	39.5
B-FM	44.11	49.61	915.00	54.61	1489.2	74.24

Table 8. Tensile strain at reinforcement

Specimen ID	f_c (MPa)	P_{max} (kN)	At maximum load		At ultimate load	
			Steel reinforcement strain (10-6) (mm/mm)	Decrease in strain (%)	Steel reinforcement strain (10-6) (mm/mm)	Decrease in strain (%)
B-R	32.23	27.66	861.0	-	1521.7	-
B-S	42.20	49.02	1607.5	86.7	3094.2	103.3
B-B	50.61	56.76	2013.9	133.9	3915.0	157.2
B-G	48.25	54.24	1879.9	118.3	3805.7	150.1
B-WP	42.40	44.82	1511.4	75.5	3011.6	97.9
B-HF	27.50	51.47	1774.3	106.0	3343.2	119.7
B-IP	51.22	32.84	1284.8	49.2	2097.7	37.8
B-IS	54.92	44.94	1529.8	77.6	3033.7	99.3
B-Y	40.83	42.07	1337.2	55.3	2235.6	46.9
B-FM	44.11	49.61	1740.7	102.1	3044.0	100.0

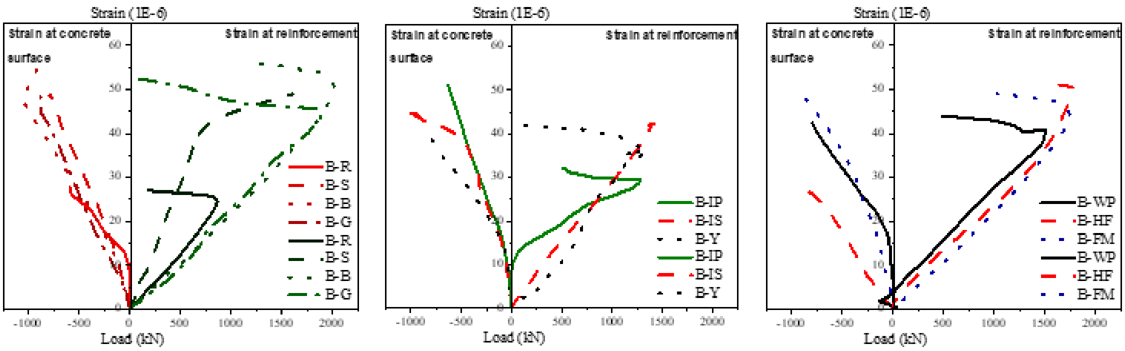

Fig. 10. Maximum load-strain at maximum load curves

Steel fibers, owing to their high elastic modulus and superior interfacial bond strength with the geopolymer matrix, significantly enhanced the reinforcement strain by improving stress transfer efficiency and delaying slip at the steel–concrete interface. This improved bond stiffness allowed the tensile reinforcement to engage more effectively under load, leading to higher strain development before yielding. In contrast, hemp fibers, characterized by their relatively low stiffness and high deformability, facilitated larger crack opening displacements and promoted distributed micro-cracking in the concrete surface. This behavior resulted in a more gradual strain evolution and higher surface strain capacity before failure, demonstrating a pronounced ductile response and improved post-cracking energy absorption.

3.4. Residual strength, toughness, toughness index, and energy dissipation capacity

In this section, the flexural strength of the tested beams on which three-point shear tests were applied, residual strength, toughness, toughness index, and energy absorption capacity, depending on the flexural strength, were evaluated. The flexural strength can be obtained by

$$f_f = \frac{3PL}{2bd^2} \quad (1)$$

where P is the recorded maximum load, b and d are the width (150 mm) and effective height (120 mm) of the beam, respectively. In accordance with ASTM C1609 [62], the maximum load (P_{max}) and the residual loads ($P_{L/400}$, $P_{L/300}$, $P_{L/150}$, and $P_{L/100}$) serve as parameters for determining the flexural strength (f_f), also referred to as the modulus of rupture, as well as the residual strengths ($f_{L/400}$, $f_{L/300}$, $f_{L/150}$, and $f_{L/100}$) of the GPC beams. These calculations correspond to specific net deflections of $L/400$, $L/300$, $L/150$, and $L/100$, which equate to 1.75 mm, 2.33 mm, 4.66 mm, and 7 mm, respectively. The flexural toughness (T_f) at various deflections ($T_{f,L/400}$, $T_{f,L/300}$, $T_{f,L/150}$, and $T_{f,L/100}$) is defined as the area under the load-deflection curve up to the specified net deflection [62]. A comprehensive summary of the results on flexural strength, residual flexural strength, and flexural toughness is presented in Table 9. Fig. 11 illustrates a typical load-deflection curve for specimens subjected to three-point bending, with L representing the span length of the beam specimens between the supports. It is also important to note that $P_{L/400}$, $P_{L/300}$, $P_{L/150}$, and $P_{L/100}$ are classified as post-cracking residual loads.

Table 9. Summary of residual strength and toughness results

Specimen ID	Max. load (P_{max}) (kN)	Flexural strength (MPa)	$f_{L/400}$ (MPa)	$f_{L/300}$ (MPa)	$f_{L/150}$ (MPa)	$f_{L/100}$ (MPa)	$T_{L/400}$ (kNmm)	$T_{L/300}$ (kNmm)	$T_{L/150}$ (kNmm)	$T_{L/100}$ (kNmm)
B-R	27.66	13.45	4.97	2.84	0.82	0.00	30.94	35.45	42.88	0
B-S	49.02	23.83	17.70	14.65	8.30	4.60	47.18	66.32	119.54	150.66
B-B	56.76	27.59	25.05	27.28	20.86	14.05	31.37	63.36	178.92	261.77
B-G	54.24	26.37	25.36	23.52	16.45	10.31	73.92	103.12	200.39	263.98
B-WP	44.82	21.79	15.01	12.90	5.94	2.94	61.32	77.89	123.36	143.29
B-HF	51.47	25.02	24.80	23.63	17.98	13.71	62.21	91.18	191.96	269.51
B-IP	32.84	15.96	10.25	7.90	2.97	1.52	46.00	56.81	80.48	91.31
B-IS	44.94	21.85	19.85	17.53	11.07	5.95	52.34	74.65	143.65	184.01
B-Y	42.07	20.45	16.05	13.70	7.52	3.46	57.05	74.32	125.39	150.07
B-FM	49.61	24.12	22.45	20.73	14.03	8.44	67.08	92.86	175.03	228.64

$f_{L/400}$, $f_{L/300}$, $f_{L/150}$, and $f_{L/100}$: residual flexural strengths at the deflections of L/400 (1.75 mm), L/300 (2.33 mm), L/150 (4.66 mm), L/100 (7 mm), respectively; $T_{L/400}$, $T_{L/300}$, $T_{L/150}$, and $T_{L/100}$: flexural toughness at the deflections of L/400, L/300, L/150, L/100, respectively.

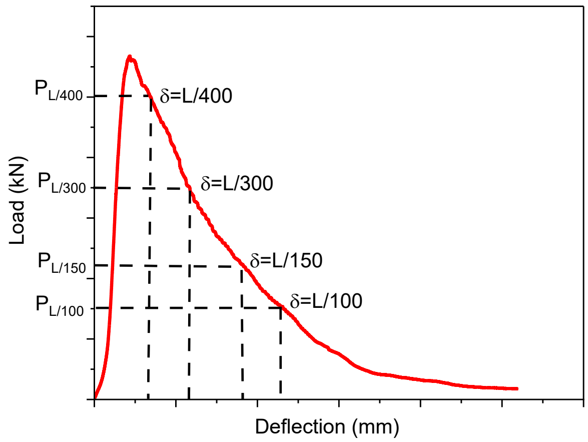

Fig. 11. Illustration of a typical load-deflection curve

The types of waste fibers used in the GPC mixture affect the residual strength and toughness, as shown in Table 9. The $L/100$ (7 mm) value of the B-R sample was determined as zero because the deflection capacity of this sample (Δ_u = 6 mm) was less than 7 mm. First of all, especially in the B-B and B-G samples, since the basalt and glass fibers provided a good compatibility with the GPC matrix, high residual strength and toughness values were achieved after cracking (post-cracking). For example, the $f_{L/300}$ and $f_{L/150}$ values in the B-B sample were 27.28 MPa and 20.86 MPa, respectively, indicating that this sample exhibited high strength even after the first crack. Similarly, the B-G sample also exhibited a similar strength trend and reached one of the highest toughness values (263.98 kN·mm, $T_{L/100}$) after first crack. On the other hand, the B-WP specimen, which showed an adequate performance with regard to shear strength, exhibited a low residual strength and toughness performance. Also, the B-HF specimen, which showed a good shear performance, exhibited a high residual strength and toughness performance. However, the residual strength results of the specimens using waste plastic and iron powder were low compared to the other specimens. In addition, the B-HF and B-FM specimens using hemp fiber and waste fabric exhibited a high performance compared to the samples with waste fiber. This situation was caused by the high deflection capacity of the B-HF specimen in particular. The B-IP specimen using iron powder exhibited a very low performance in terms of toughness value. Similarly, the low deflection capacity of the B-IP specimen caused this situation. In general, it is seen that the fiber types used in the GPC mixture have an effect on the results of post-cracking toughness and residual strength. Although the specimens in which industrial fibers such as B-B and B-G with high shear performance were used also had high residual strength and toughness capacity, the residual strength and toughness performance of the samples in which fibers such as waste yarn and waste plastic were used remained at lower levels. This situation depends on the relationship between the waste fibers and the microstructure of the GPC matrix (such as the proper and homogeneous distribution of the fibers in the matrix, the binding capacity to the matrix, and sufficient load transfer). Therefore, it is seen that the ideal selection of the waste fiber type is important for the structural elements in terms of residual strength and toughness.

The incorporation of hemp and fabric fibers significantly altered the post-cracking behavior by promoting the formation of numerous closely spaced micro-cracks rather than a few dominant macro-cracks. This distributed cracking pattern enhanced the crack-bridging mechanism, where the flexible and ductile nature of these fibers allowed them to bridge developing cracks and sustain tensile stresses even after matrix cracking. As a result, sudden load drops were effectively mitigated, leading to a more stable and gradual post-peak load–deflection response with improved energy absorption and deformation capacity. In contrast, steel and basalt fibers, due to their high elastic modulus, superior tensile strength, and strong interfacial bond with the geopolymer matrix, played a critical role in maintaining load-carrying capacity beyond the peak load. These fibers effectively transferred stresses across widened cracks, delayed crack propagation, and provided additional restraint against crack opening, which not only preserved the structural integrity of the beams but also extended the post-yield deformation range. Consequently, beams reinforced with steel and basalt fibers exhibited a pronounced strain-hardening response, higher residual strength, and enhanced ductility, indicating their effectiveness in sustaining significant loads during the post-cracking phase.

In Fig. 12, the normalized flexural strength, flexural toughness index (I_f), energy dissipation capacity, and the interrelation between normalized flexural strength and both flexural strength and energy dissipation capacity are presented. To mitigate the effects of compressive strength, the normalized flexural strengths of the specimens are calculated using the formula $f_f/\sqrt{f_c}$ [63]. The I_f can be described as the ratio of the toughness of fiber-reinforced concrete to that of standard concrete without fibers [63]. Moreover, the energy dissipation capacity of the tested specimens is assessed by evaluating the area under the load-displacement curve.

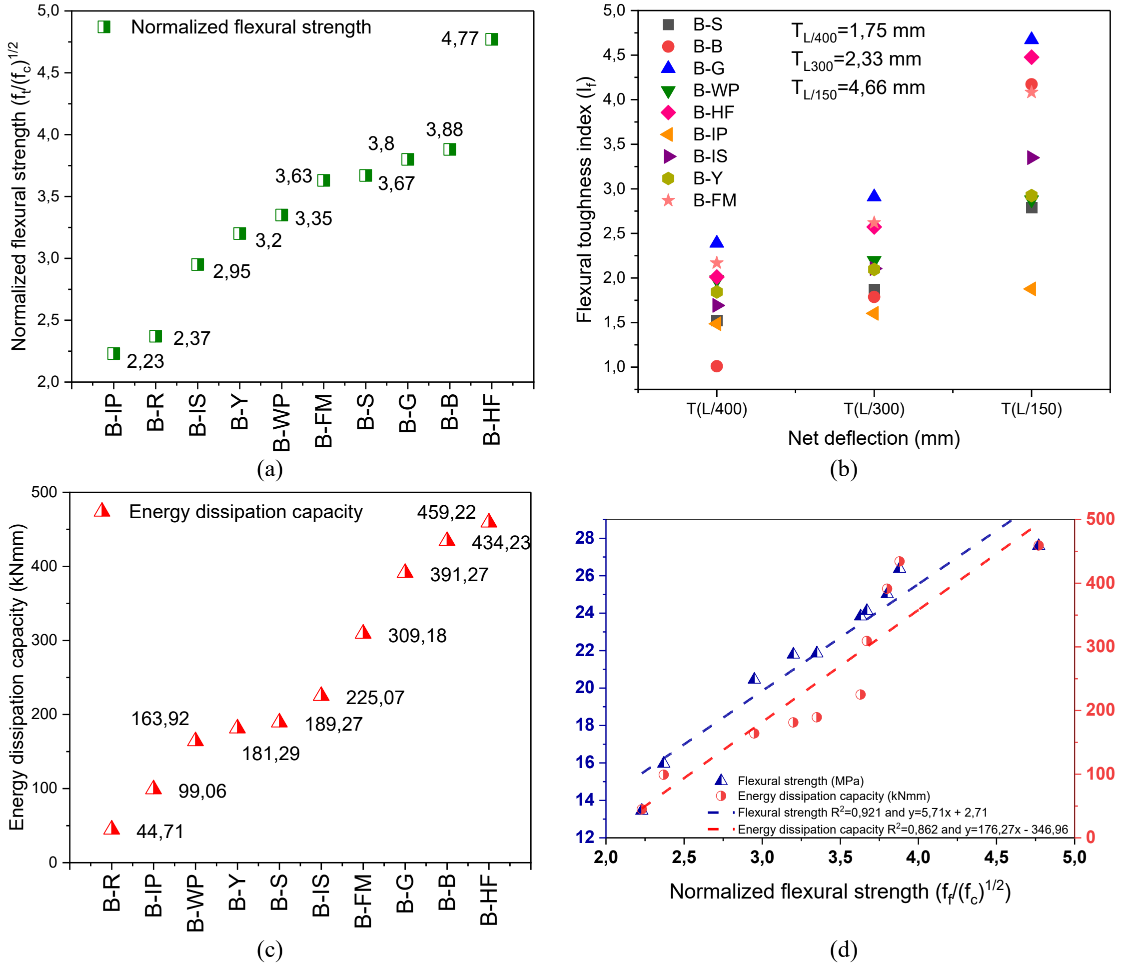

Fig. 12. Comparison of (a) normalized flexural strength, (b) flexural toughness index, (c) energy dissipation capacities, and (d) relationship between normalized flexural strength and flexural strength, energy dissipation capacity

The highest energy absorption capacity (E) was achieved in B-B and B-G specimens using basalt and glass fiber. The deflection capacity of these specimens was higher than the other specimens, except the B-HF sample, and had a high shear force capacity, which affected E. The deflection capacity increased due to the fact that glass and basalt fibers were embedded in the GPC matrix and were effective in resisting the principal tensile stresses and crack formation. In addition, the loss of strength after the maximum load in these samples was slower than in other samples.

It should be noted that the E values of B-HF, B-FM, and IS specimens were higher than B-S specimen. Although the use of steel fiber had a significant effect on the shear strength capacity, its effect on the displacement capacity was less. In particular, although the shear force capacities of B-HF and B-FM specimens were lower than B-S specimen, the displacement capacity (Δ_u) of B-HF and B-FM specimens were 1.77 and 1.23 times higher than B-S specimen, respectively. The higher displacement capacity of these specimens caused an increase in E values.

The displacement capacity of the specimen has also increased due to the more elastic behavior of hemp fiber and waste fabric fiber in the matrix. However, although the utilization of steel increased the shear strength with a bridging effect, it did not have a significant effect on the displacement capacity. The minimum E value was reached in the B-IP specimen. The waste iron powder in the GPC mixture did not have a significant effect on the displacement capacity and, therefore, on E. The waste iron powder in the mixture, being in powder form, neither affected the crack distribution nor allowed the beam to deflect since it did not have elastic ability.

However, all of the beams without stirrups have higher E values compared to the reference specimen. In other words, the application of waste materials as fibers within the recycling framework of GPC has been shown to be effective, particularly in relation to the E value. It is also observed that a linear relationship exists between the flexural strength and the ability to absorb energy. As the flexural strength increases, the energy absorption capacity of the beams also increases.

Variations in the fiber type utilized in the GPC mixture affect the energy absorption capacity after a fracture occurs. In addition, the regression line between the ff and E shows that the relationship between these two parameters is strong. It is seen with the value of $R^2 = 0.862$ that the effect of the increase in the flexural strength of the specimen on the energy absorption capacity is high. In this case, the addition of both industrial and waste fibers to the GPC mixture slowed down the crack propagation of the beam and increased the E values.

3.5. Comparisons with code provisions

This section presents a comparison between the experimental outcomes of RSGC beams and the theoretical shear strength values suggested by the relevant codes. In general, international standards recommend theoretical formulas for estimating both the flexural and shear capacity of beams with stirrups. However, there are also theoretical formulas recommended by the relevant standards/codes for the shear capacity of beams without stirrups. This paper considers several codes, including ACI318-19 [53], Eurocode-2 [64], Italian code DM 204 [65], fib Model Code 2020 approach [66], Swiss code SIA 262 [67], Canadian standard CSA A23.3.04 [68], Japanese standard JSCE [69], British standard BS8110–1 [70], and Australian standard AS 3600 [71]. The theoretical shear capacity formulas recommended by the relevant standards/codes for beams without stirrup are presented in Table 10. The parameters used in the formulas recommended by the standards for the shear capacity of beams without stirrup are also presented in Table 11.

Table 10. Formulas recommended by standards/codes for the shear capacity of a beam without stirrup

Standard	Formula
ACI318-19 [53]	$V_{Rd} = 0.17\sqrt{f_{ck}}b_w d$
Eurocode -2 [64]	$V_{Rd} = max\left\{\begin{matrix}\left(\frac{(0.18k(100\rho_l f_{ck})^{1/3}}{\gamma_c} + 0.15\sigma_{cp}\right)b_w d \\ (v_{min} + 0.15\sigma_{cp})b_w d\end{matrix}\right\}$ $v_{min} = 0.035kf_{ck}^{1/2};\ k = 1 + (200/d)^{1/2}$
fib Model Code 2020 [66] & Australian code AS3600 [71]	$V_{Rd} = k_v\frac{\sqrt{f_{ck}}}{\gamma_c}b_w d$ LoA I: $k_v = \frac{0.40}{(1 + 750f_{yd}/E_s)}\frac{1300}{(1000 + 1.25d)}$ LoA II: $k_v = \frac{0.40}{(1 + 1500\varepsilon_x)}\frac{1300}{(1000 + K_{dg}d)}$ $K_{dg} = \frac{32}{16 + d_{max}} \geq 0.75;\ \varepsilon_x = \frac{1}{2E_s A_s}\left(\frac{M_{Ed}}{d} + V_{Ed} + \frac{1}{2}N_{Ed} \geq 0\right)$

Table 10. Continued

Standard	Formula
Swiss code SIA 262 [67]	$V_{Rd} = \frac{0.3\sqrt{f_{ck}}db_w}{\gamma_c(1+\varepsilon_v dk_g)}$
Italian DM 204 [65]	$V_{Rd} = \frac{0.3\sqrt{f_{ck}}db_w}{\gamma_c(1+0.0022_v d)}$
Canadian code A23.3.04 [68]	$V_{Rd} = \lambda\beta\sqrt{f_{ck}}b_w d\beta$
Japanese code JSCE [69]	$V_{Rd} = \beta_d\beta_p f_{vcd} b_w d$ $\beta_b = \sqrt[4]{1000/d} \leq 1.5;\ \beta_p = \sqrt[3]{100\rho_l} \leq 1.5;\ f_{vcd} = 0.2\sqrt[3]{f_{ck}} \leq 0.72$
British code BS8110-1 [70]	$V_{Rd} = 0.79\left(100\frac{A_s}{b_w d}\right)^{1/3}\left(\frac{400}{d}\right)^{1/4}\left(\frac{f_{ck}}{25}\right)^{1/3} b_w d$

Table 11. Parameters of shear capacity formulas recommended by standards/codes

	ACI	EU	fib MC 2020		SIA 262	DM 204	A23.3	JSCE	BS81110-1
			LoA I	LoA II AS3600					
d	+	+	+	+	+	+	+	+	+
b_w	+	+	+	+	+	+	+	+	+
ρ_l		+						+	+
f_{ck}	+	+	+	+	+	+	+	+	+
fyk			+		+				
V_{ed}				+					
M_{ed}				+	+				
N_{ed}				+					
E_s			+	+	+				
As				+					
d_{max}					+				
k		+							
ε_x				+	+				
β							+	+	

Experimental and theoretical shear capacity results are presented in Fig. 13. The relationship between experimental and theoretical shear capacity recommended by standards/codes is also presented in Fig. 14. Since the B-B beam has stirrups, the experimental and theoretical results of the B-B specimen are not compared with other specimens in this section. The theoretical shear capacity recommended by the standards/codes for beams without stirrups is lower compared to the experimental results. It should also be noted that the concrete compressive strength of OPC and 28-day compressive strength in the formulas suggested by the relevant standards/codes were taken into account. However, in this study, the GPC and 7-

day early compressive strength results were used in the relevant standards/codes. The comparison of experimental and theoretical shear capacity results of tested beams is shown in Table 12.

The theoretical shear force results suggested by the Eurocode-2 standard are higher than the experimental results. Although there is an average difference of 54% between the theoretical and experimental shear capacity of beams where industrial fibers (glass, basalt, and steel) are used, this difference is 59% on average in beams where waste fibers are used. The reason for this is that the Eurocode-2 standard takes into account the beam geometry, concrete compressive strength, and longitudinal reinforcement ratio parameters for shear capacity.

The fib model LoA I and LoA II codes (also AS3600) are quite inadequate in predicting the shear force capacity of beams without stirrups. Although there is an average difference of 220% and 184%, respectively, between the theoretical and experimental results of industrial and waste fiber beams in the LoA I approach, this ratio increases to 636% and 442%, respectively, in the LoA II approach. In particular, although the fib model LoA II code approach takes into account many factors for the theoretical shear force capacity, the difference between the theoretical and experimental results is quite high. It is thought that the reason for this situation is the difference between the compressive strengths of the waste fibers and the beam shear force strength. For example, although the compressive strength of the hemp fiber sample is 27.50 MPa, the shear capacity of the tested beam is 51.47 kN. Since the compressive strength is taken into account for the theoretical shear capacity in the fib model code approach, there are significant differences.

The Swiss SIA 262 code and Italian DM 204 standards were also inadequate in predicting the shear capacity of both industrial and waste fiber beams. The theoretical results suggested by these two regulations are also close to each other. There are also significant differences between the theoretical and experimental shear capacity suggested by the Japanese JSCE and British BS81110-1 standards. Since these two regulations take into account similar parameters for theoretical shear capacity, the results are close to each other.

When the theoretical shear capacity suggested by ACI318 for beams without stirrups is compared with the experimental results, it gives closer results than other standards/codes, except A23.3. However, ACI318 is still insufficient to estimate the experimental shear capacity of beams with industrial fibers (glass, basalt, and steel fibers). The experimental shear capacity of B-B, B-S, and B-G specimens is approximately 50% higher than the theoretical result. Similarly, the ACI318 standard is also insufficient to estimate the shear capacity of waste fiber specimens. There is an average difference of 46% between the experimental and theoretical shear capacity of other samples except the B-IP specimen. In this case, this is because the formula suggested by the ACI standard for shear capacity only takes into account the beam geometric parameters, b_w and d, and the concrete compressive strength, f_{ck}.

The closest results between the experimental and theoretical shear capacity results were obtained in the Canadian A.23.3 code. The theoretical shear capacity suggested by the A.23.3 code is 38% and 22% less than the experimental shear capacity of industrial fiber and waste fiber specimens, respectively. These rates are the closest results between the experimental and theoretical results. This situation is because the A.23.3 code takes into account both the β values and the formula $f_{cd} = 0.2\sqrt[3]{f_{ck}} \leq 0.72$. With the beta values, the effects of the geometric and longitudinal reinforcement ratio of the beam, and the formula $f_{cd} = 0.2\sqrt[3]{f_{ck}} \leq 0.72$, and the concrete compressive strength on the theoretical shear capacity was reduced. Thus, the differences between the theoretical and experimental shear capacities were reduced.

Although the theoretical shear capacity suggested by the Eurocode-2 standard for beams without stirrups is higher than the experimental results, the theoretical results suggested by other standards/codes are lower than the experimental results. When evaluated in general, although waste fibers in particular significantly increase the tensile strength of GPC and thus limit the crack distribution, the tensile strength of concrete was not taken into account in the theoretical formulas. This caused a difference between the theoretical and experimental results.

It should be noted that the observed enhancement in apparent tensile response is associated with fiber bridging and stress redistribution at the beam level rather than an intrinsic increase in matrix tensile strength. The specimen geometry and the three-point bending configuration contributed to this localized strengthening behavior, highlighting the role of fibers in crack arrest and load transfer mechanisms.

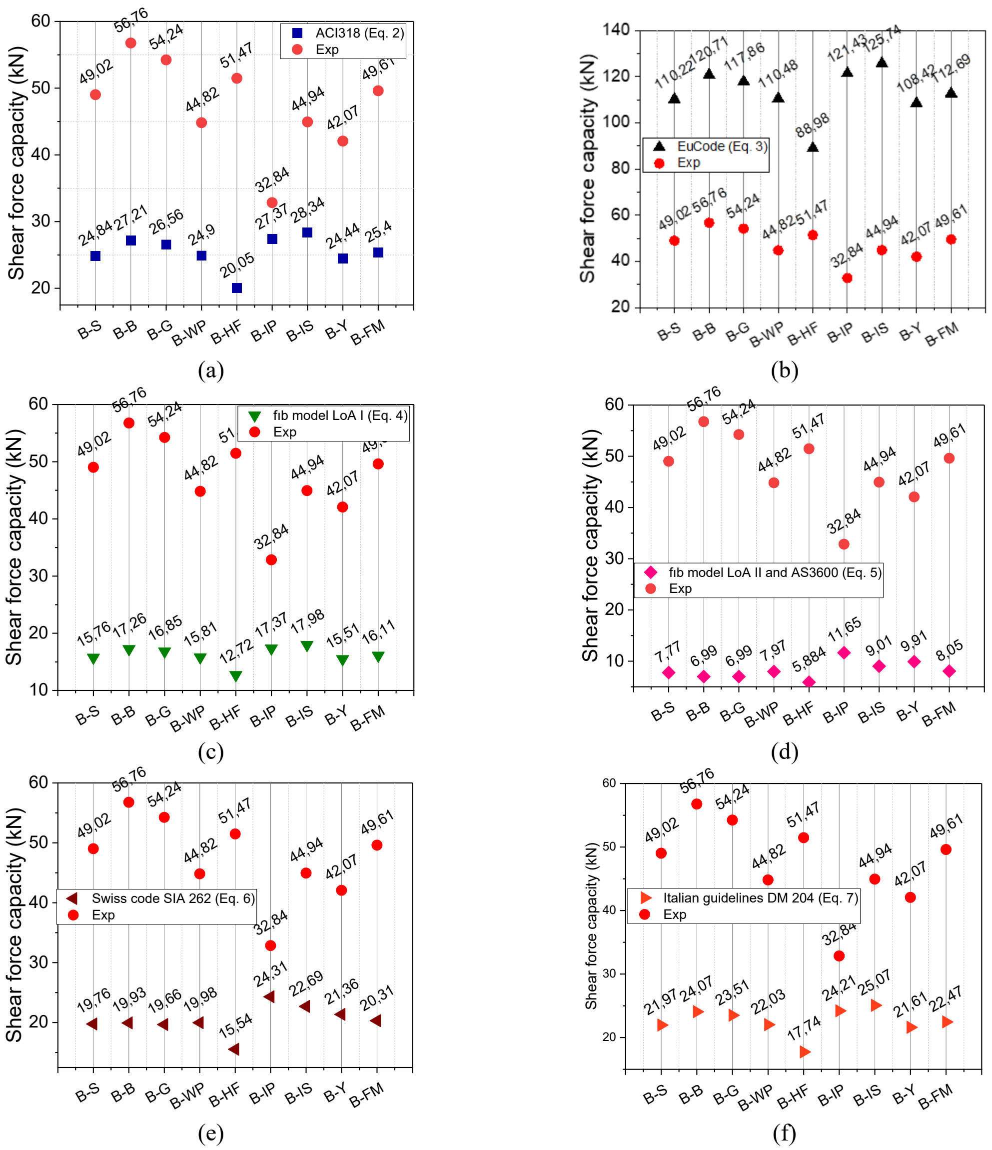

Fig. 13. Experimental and theoretical cutting force capacity results: (a) ACI318-19, (b) Eurocode-2, (c) fib model code LoA I, (d) fib model code LoA II, and AS3600, (e) Swiss code SIA262 (f) Italian code DM204, (g) Canadian code A23.3.04, (h) Japanese code JSCE, (i) British code BS81110-0

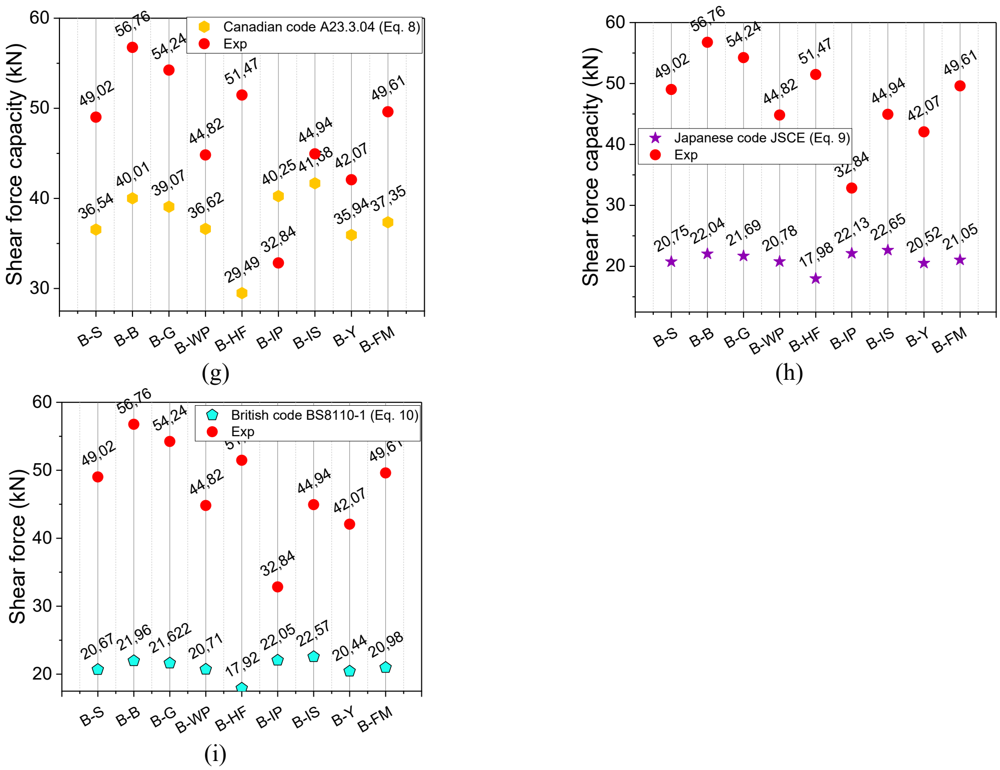

Fig. 13. Continued

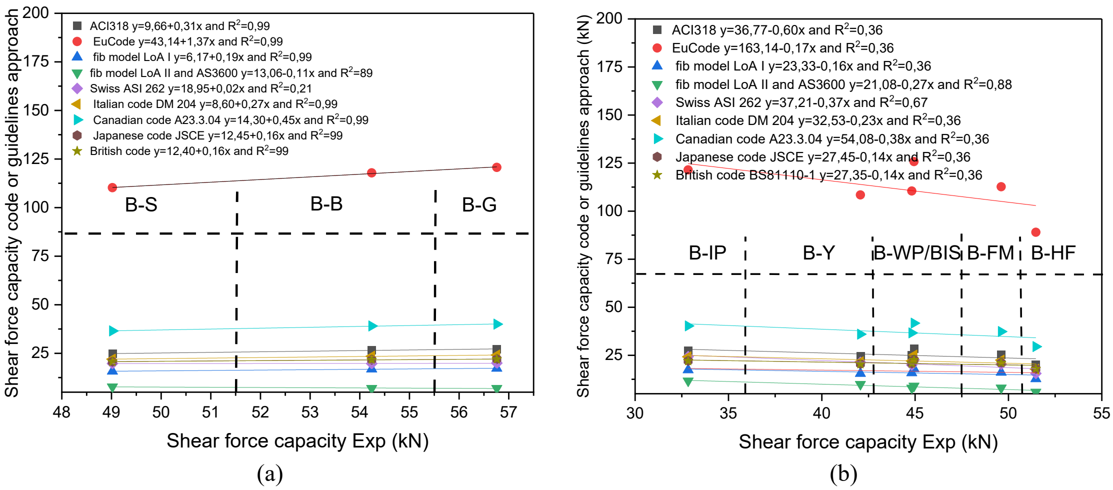

Fig. 14. Relationship between experimental and theoretical shear capacity results of tested beams with (a) steel, glass, and basalt fiber, (b) waste fibers

Table 12. Comparison of experimental and theoretical shear capacity results of tested beams

Beam	Exp.	ACI	Increase in shear capacity %	EU	Increase in shear capacity %	fib model code 2020		Increase in shear capacity %	Increase in shear capacity %
						LoA I	LoA II AS3600		
B-S	49.02	24.85	49.31	110.23	-55.53	15.77	7.78	210.90	530.26
B-B	56.76	27.21	52.06	120.71	-52.98	17.27	6.99	228.72	711.83
B-G	54.24	26.57	51.02	117.87	-53.98	16.86	6.99	221.72	675.59
B-WP	44.82	24.91	44.43	110.49	-59.44	15.80	7.97	183.59	462.29
B-HF	51.47	20.06	61.03	88.98	-42.16	12.73	5.89	304.38	774.05
B-IP	32.84	27.37	16.64	121.44	-72.96	17.37	11.66	89.06	181.71
B-IS	44.94	28.35	36.92	125.75	-64.26	17.99	9.02	149.85	398.35
B-Y	42.07	24.44	41.90	108.42	-61.20	15.51	9.91	171.26	324.36
B-FM	49.61	25.40	48.79	112.70	-55.98	16.12	8.06	207.76	515.57
B-S	49.02	19.76	148.03	21.98	123.03	36.54	34.15	20.75	136.24
B-B	56.76	19.93	184.78	24.07	135.81	40.02	41.84	22.05	157.46
B-G	54.24	19.67	175.78	23.50	130.79	39.07	38.82	21.70	149.98
B-WP	44.82	19.98	124.29	22.03	103.44	36.63	22.37	20.78	115.66
B-HF	51.47	15.55	231.02	17.74	190.09	29.50	74.49	17.99	186.10
B-IP	32.84	24.31	35.09	24.21	35.62	40.26	-18.42	22.13	48.37
B-IS	44.94	22.69	98.06	25.07	79.23	41.69	7.81	22.65	98.37
B-Y	42.07	21.36	96.95	21.62	94.59	35.94	17.05	20.52	104.99
B-FM	49.61	20.31	144.23	22.47	120.77	37.36	32.79	21.06	135.58

4. Conclusion

This study aims to evaluate waste materials (yarn, fabric, hemp, plastic, iron powder, and iron shavings) as an alternative shear reinforcement in beams without stirrups. The six GPC beams without stirrup (containing waste fibers) and three GPC beams without stirrup (containing steel, glass, and basalt fibers), and one GPC beam with stirrup as a reference, were cast and tested under a three-point bending test. All beams were 150 mm wide and 150 mm deep with lengths of 750 mm. The results were analyzed and discussed in terms of load-midpoint deflection curves, crack pattern, failure mode, load-strain curve, peak strain (strain corresponding to peak stress), residual strengths, toughness, and toughness index. Finally, the experimental shear resistance is compared to the estimated shear resistance computed using the available beam without stirrup design code equations in ACI318-19, Eurocode-2, Italian code DM 204, fib Model Code 2020 approach, Swiss code SIA 262, Canadian standard CSA A23.3.04, Japanese standard JSCE, British standard BS8110–1, and Australian standard AS 3600. The outcomes achieved in this research can be succinctly outlined as follows:

1. Both industrial fibers (steel, glass, and basalt) and waste fibers had a positive effect on the weak tensile strength of GPC, preventing the propagation of diagonal tensile cracks and increasing the shear capacity of the tested beams. However, this effect varied due to the fiber type and the interaction of the fibers with the GPC matrix. Although the shear strength of beams using industrial fibers is 77%

to 105% higher compared to the reference specimen, this ratio varies between 18% and 86% in beams containing waste fiber. Although the shear strength of the sample using iron powder was the lowest when compared to fiber beams, hemp fiber stands out as an ideal waste material as an alternative to shear reinforcement.

2. The strain of the concrete surface and longitudinal reinforcement was affected by the use of industrial and waste fibers. However, both strains of concrete surface and strain of rebar increased with industrial fibers compared to the specimens with waste fibers. Especially the use of basalt, glass, and steel fibers caused the strain in the reinforcement to increase more than two times compared to the reference sample.
3. The energy dissipation capacity of the tested beams increased substantially by using both industrial and waste fibers. The test results confirmed that waste hemp fiber and waste fabric material recovered from tires are suitable for GPC production in terms of dissipation capacity. The using steel, basalt, and glass fibers, especially B-B and B-G specimens, led to good compatibility with the GPC matrix, high residual strength, and toughness values after post-cracking. However, although using waste plastic had a positive effect on the shear strength, the residual strength and toughness of B-WP beams decreased. Both residual strength and toughness of B-HF increased by up to 38-88% with the addition of hemp fiber.
4. Hemp fiber addition increased the shear capacity by up to 86% compared to the reference beam. The residual strength of basalt fiber-reinforced beams was 0.85 P_{max}, approximately 40% higher than the control specimen. The ultimate deflection of specimens containing fabric fibers increased by 65%, indicating a significant improvement in ductility and deformation capacity. The energy absorption capacity of hemp fiber-reinforced beams was approximately 2.3 times greater than that of the reference specimen, demonstrating the effectiveness of natural fibers in enhancing post-cracking performance. The toughness index (I_{10}) of steel fiber-reinforced beams increased from 2.1 in the control beam to 4.5, confirming a substantial enhancement in post-peak energy dissipation behavior.
5. The improvement in shear strength was closely related to the tensile and geometric characteristics of the waste materials. High-aspect-ratio and high-tensile-strength fibers such as hemp and fabric fibers significantly enhanced the matrix's crack-bridging ability, leading to shear strength gains of up to 75–86% compared to the reference beam. In contrast, granular or non-fibrous wastes such as iron powder and waste plastic exhibited only limited improvements, typically below 20–30%, due to their insufficient aspect ratio and weak mechanical interlocking with the geopolymer matrix. These findings confirm that the efficiency of waste inclusions in shear strengthening is primarily governed by their geometry, aspect ratio, and interfacial bonding characteristics.
6. The empirical relationships utilized to compute shear resistances in multiple design codes—namely ACI 318-19, fib Model Code 2020, AS 3600 (Australia), SIA 262 (Switzerland), DM 204 (Italy), CSA A23.3-04 (Canada), JSCE (Japan), and BS8110-1 (UK)—have been found to underestimate the experimental shear resistance of GPC beams without stirrups, except Eurocode-2.

Declaration of conflicting interests

The author(s) declared no potential conflicts of interest with respect to the research, authorship, and/or publication of this article.

Funding

No funding was received for this study.

Data availability statement

The data that support the findings of this study are available from the corresponding author upon reasonable request.

Nomenclature

A_c	:	Cross-section
A_s	:	Area of the longitudinal reinforcement (mm^2)
b_w	:	Minimum width of the cross section (mm);
d	:	Effective depth of the cross section (mm);
E_s	:	Young's modulus of longitudinal reinforcement
f_{ck}	:	Characteristic value of the cylindrical compressive strength of the concrete (MPa)
f_{cd}	:	$= f_{ck} / \gamma_c$, the design cylindrical compressive strength of the concrete (MPa)
f_{yd}	:	Yielding stress of steel (MPa)
d_{max}	:	Aggregate size
k	:	Shape factor
k_v	:	Signifies the capacity of cracked concrete
M_{Ed}	:	Bending moment
N_{Ed}	:	Axial compressive load
V_{Ed}	:	Shear force
V_{Rd}	:	Shear capacity
ε_x, ε_v	:	Longitudinal strain
ρ_l	:	Longitudinal reinforcement ratio
γ_c	:	=1.5, the partial safety factor of the concrete
σ_{cp}	:	$= N_{Ed} / A_c$ (MPa) $\leq 0.2\ f_{cd}$: the mean prestressing stress acting in the cross section
λ	:	Dimensionless factor (1 for normal-density concrete)
β	:	Coefficient that defines the width of the strut as a function of the effective depth d of the section, generally assumed in the range 0.2–0.3

References

[1] Abbass M, Singh G (2023) Experimental investigation of alkali-activated hybrid geopolymer concrete. Multiscale Multidiscip Model Exp Des 1–15. https://doi.org/10.1007/s41939-023-00144-1

[2] Chen C, Habert G, Bouzidi Y, Jullien A (2010) Environmental impact of cement production: detail of the different processes and cement plant variability evaluation. J Clean Prod 18(5):478–485. https://doi.org/10.1016/j.jclepro.2009.12.014

[3] Meyer C (2009) The greening of the concrete industry. Cem Concr Compos 31(8):601–605. https://doi.org/10.1016/j.cemconcomp.2008.12.0100,

[4] Gartner E (2004) Industrially interesting approaches to “low-CO2” cements. Cem Concr Res 34(9):1489–1498. https://doi.org/10.1016/j.cemconres.2004.01.021

[5] Rajendran M, Bakthavatchalam K, Leela Bharathi S (2023) Review on the hybridized application of natural fiber in the development of geopolymer concrete. J Nat Fibers 20(1):2178578. https://doi.org/10.1080/15440478.2023.2178578

[6] Marvila MT, Rocha HA, de Azevedo ARG, Colorado HA, Zapata JF, Vieira CMF (2021) Use of natural vegetable fibers in cementitious composites: Concepts and applications. Innov Infrastruct Solut 6:1–24. https://doi.org/10.1007/s41062-021-00551-8

[7] Rashad AM (2013) A comprehensive overview about the influence of different additives on the properties of alkali-activated slag–A guide for civil engineer. Constr Build Mater 47:29–55. https://doi.org/10.1016/j.conbuildmat.2013.04.011

[8] Hassan A, Arif M, Shariq M (2019) Use of geopolymer concrete for a cleaner and sustainable environment–A review of mechanical properties and microstructure. J Clean Prod 223:704–728. https://doi.org/10.1016/j.jclepro.2019.03.051
[9] Aliabdo AA, Abd Elmoaty M, Emam MA (2019) Factors affecting the mechanical properties of alkali activated ground granulated blast furnace slag concrete. Constr Build Mater 197:339–355. https://doi.org/10.1016/j.conbuildmat.2018.11.086
[10] Ng C, Alengaram UJ, Wong LS, Mo KH, Jumaat MZ, Ramesh S (2018) A review on microstructural study and compressive strength of geopolymer mortar, paste and concrete. Constr Build Mater 186:550–576. https://doi.org/10.1016/j.conbuildmat.2018.07.075
[11] Ma C-K, Awang AZ, Omar W (2018) Structural and material performance of geopolymer concrete: A review. Constr Build Mater 186:90–102. https://doi.org/10.1016/j.conbuildmat.2018.07.111
[12] Arioz O, Bzeni DK, Zangy RR, Arioz E (2020) Properties of slag-based geopolymer pervious concrete for ambient curing condition. In: Proceedings of the IOP Conference Series: Materials Science and Engineering. IOP Publishing.
[13] Gopalakrishnan R, Chinnaraju K (2019) Durability of ambient cured alumina silicate concrete based on slag/fly ash blends against sulfate environment. Constr Build Mater 204:70–83. https://doi.org/10.1016/j.conbuildmat.2019.01.153
[14] Lakew AM, Canpolat O, Al-Mashhadani MM, Uysal M, Niş A, Aygörmez Y, Bayati M (2023) Combined effect of using steel fibers and demolition waste aggregates on the performance of fly ash/slag based geopolymer concrete. Eur J Environ Civ Eng 1–28. https://doi.org/10.1080/19648189.2023.2189468
[15] Farhan KZ, Megat AMJ, Demirboğa R (2023) Performance of polypropylene fiber reinforced GGBFS-based alkali activated composites under sulfate and freeze–thaw conditions. Mater Struct 56(2):44. https://doi.org/10.1617/s11527-023-02137-5
[16] Afroughsabet V, Ozbakkaloglu T (2015) Mechanical and durability properties of high-strength concrete containing steel and polypropylene fibers. Constr Build Mater 94:73–82. https://doi.org/10.1016/j.conbuildmat.2015.06.051
[17] Ganesan N, Indira P, Sabeena M (2013) Tension stiffening and cracking of hybrid fiber-reinforced concrete. ACI Mater J 110(6).
[18] Dawood ET, Ramli M (2014) The effect of using high strength flowable system as repair material. Compos Part B Eng 57:91–95. https://doi.org/10.1016/j.conbuildmat.2009.11.013
[19] Banthia N, Majdzadeh F, Wu J, Bindiganavile V (2014) Fiber synergy in hybrid fiber reinforced concrete (HyFRC) in flexure and direct shear. Cem Concr Compos 48:91–97. https://doi.org/10.1016/j.cemconcomp.2013.10.018
[20] Yang K-H (2011) Tests on concrete reinforced with hybrid or monolithic steel and polyvinyl alcohol fibers. ACI Mater J 108(6).
[21] Zhou J, Kang T, Wang F (2019) Pore structure and strength of waste fiber recycled concrete. J Eng Fibers Fabr 14:1558925019874701. https://doi.org/10.1177/1558925019874701
[22] Jinghai Z, Tianbei K, Fengchi W (2020) The permeability of waste fiber recycled concrete. Mater Sci 26(2):210–217. http://dx.doi.org/10.5755/j01.ms.26.2.21143
[23] Zhou JH, Kang TB, Wang FC, Dong W (2016) Experimental study on fracture properties of waste fiber recycled concrete. In: Proceedings of the MATEC Web of Conferences. EDP Sciences, France.
[24] Colombo B, Gaiardelli P, Dotti S, Caretto F, Coletta G (2021) Recycling of waste fiber-reinforced plastic composites: a patent-based analysis. Recycling 6(4):72. https://doi.org/10.3390/recycling6040072
[25] Tran TT, Pham TM, Hao H (2019) Experimental and analytical investigation on flexural behaviour of ambient cured geopolymer concrete beams reinforced with steel fibers. Eng Struct 200:109707. https://doi.org/10.1016/j.engstruct.2019.109707
[26] Shelton JJ, Naresh YV, Solomon AA, Daniel C (2021) Experimental and analytical investigation of geo-grid confined RC beams with glass fiber reinforced concrete. Struct 34:487–497. https://doi.org/10.1016/j.istruc.2021.08.002
[27] Murad Y, Abdel-Jabbar H (2022) Shear behavior of RC beams prepared with basalt and polypropylene fibers. Case Stud Constr Mater 16:e00835. https://doi.org/10.1016/j.cscm.2021.e00835
[28] Wu Y (2002) Flexural strength and behavior of polypropylene fiber reinforced concrete beams. J Wuhan Univ Technol Mater Sci Ed 17(2):54–57. https://doi.org/10.1007/BF02832623

[29] Aldemir A, Akduman S, Kocaer O, Aktepe R, Sahmaran M, Yildirim G, Ashour A (2022) Shear behaviour of reinforced construction and demolition waste-based geopolymer concrete beams. J Build Eng 47:103861. https://doi.org/10.1016/j.jobe.2021.103861
[30] Wu C, Hwang HJ, Shi C, Li N, Du Y (2020) Shear tests on reinforced slag-based geopolymer concrete beams with transverse reinforcement. Eng Struct 219:110966. https://doi.org/10.1016/j.engstruct.2020.110966
[31] Madheswaran CK, Ambily PS, Lakshmanan N, Dattatreya JK, Sathik SJ (2014) Shear behavior of reinforced geopolymer concrete thin-webbed t-beams. ACI Mater J 111(1):89.
[32] Visintin P, Ali MM, Albitar M, Lucas W (2017) Shear behaviour of geopolymer concrete beams without stirrups. Constr Build Mater 148:10–21. https://doi.org/10.1016/j.conbuildmat.2017.05.010
[33] Maranan GB, Manalo AC, Benmokrane B, Karunasena W, Mendis P, Nguyen TQ (2018) Shear behaviour of geopolymer-concrete beams transversely reinforced with continuous rectangular GFRP composite spirals. Compos Struct 187:454–465. https://doi.org/10.1016/j.compstruct.2017.12.080
[34] Abdullah M, Qazi AU, Khan QS, Kazmi SMS, Munir MJ (2024) Experimental and analytical investigations on shear performance of ambient-cured reinforced geopolymer concrete beams. Buildings 14(1):204. https://doi.org/10.3390/buildings14010204
[35] Hussein MJ, Mayyahi TH, Domat WB (2024) Numerical study of shear behavior of geopolymer concrete beam without stirrups. Civil Environ Eng 20(1):526–543. https://doi.org/10.2478/cee-2024-0040
[36] Chen Y, Zhang W, Zhang Y, Liu Z, Liu C, Zhang Y, Chen M (2025) A novel in-process rebar integration method for 3D printing reinforced concrete beams and performance evaluation. Virtual Phys Prototyp 20(1):e2536556. https://doi.org/10.1080/17452759.2025.2536556
[37] Zhu J, Li S, Sun Y, Li P, Chen X, Casas JR (2025) Experimental and numerical studies on shear failure behavior variability in RC beams without shear reinforcement. Eng Fail Anal 109978. https://doi.org/10.1016/j.engfailanal.2025.109978
[38] Jia P, Wu H, Yin Z, Ma L, Huang T (2025) Mesoscopic analysis on size effect of dynamic shear response of RC beams under low-velocity impact. Int J Impact Eng 105429. https://doi.org/10.1016/j.ijimpeng.2025.105429
[39] Lin C, Shi Z, Kanstad T, Ji G (2025) Effect of high performance composite macrofiber on the shear behavior of reinforced beams without stirrups. Compos Struct 370:119406. https://doi.org/10.1016/j.compstruct.2025.119406
[40] Rasheed MHF, Taha BO, Agha AZS, Arbili MM, Abdulrahman PI (2025) Shear capacity of FRP–reinforced RC beams without stirrups: comparative modeling with FRP modulus, longitudinal ratio, and shear span-to-depth. J Compos Sci 9(10):554. https://doi.org/10.3390/jcs9100554
[41] Resende TL, Pacheco DD, Cardoso DC, Noël M (2025) Analysis of the shear behavior of GFRP reinforced concrete beams through crack kinematics and shear transfer mechanisms. Eng Struct 340:120778. https://doi.org/10.1016/j.engstruct.2025.120778
[42] ASTM C989/C989M-14 (2014) Standard specification for slag cement for use in concrete and mortars. ASTM International, West Conshohocken, PA. http://dx.doi.org/10.1520/C0989_C0989M-14
[43] Kaplan G, Öz A, Bayrak B, Aydın AC (2023) Effect of geopolymer slurries with clinker aggregates and marble waste powder on embodied energy and high-temperature resistance in prepacked concrete: ANFIS-based prediction model. J Build Eng 67:105987. https://doi.org/10.1016/j.jobe.2023.105987
[44] da Silveira Maranhão F, de Souza Junior FG, Soares P, Alcan HG, Çelebi O, Bayrak B, Aydın AC (2023) Physico-mechanical and microstructural properties of waste geopolymer powder and lime-added semi-lightweight geopolymer concrete: Efficient machine learning models. J Build Eng 72:106629. https://doi.org/10.1016/j.jobe.2023.106629
[45] Kaplan G, Shi J, Öz A, Bayrak B, Dheyaaldin MH, Aydın AC (2023) Preparation and characterization of a novel prepacked aggregate geopolymer: A feasibility study. Powder Technol 421:118423. https://doi.org/10.1016/j.powtec.2023.118423
[46] Bayrak B, Çelebi O, Öz A, Ustabaş İ, Kaplan G, Aydın AC (2023) Effect of aluminosilicate precursors and curing regime on physico-mechanical durability and microstructural characteristics of coral geopolymers (Cor-Geo): Cleaner production for coral islands. Constr Build Mater 407:133596. https://doi.org/10.1016/j.conbuildmat.2023.133596

[47] Öz A, Bayrak B, Kaplan G, Aydın AC (2023) Effect of waste colemanite and PVA fibers on GBFS-metakaolin based high early strength geopolymer composites (HESGC): Mechanical, microstructure and carbon footprint characteristics. Constr Build Mater 377:131064. https://doi.org/10.1016/j.conbuildmat.2023.131064
[48] ASTM C1437-15 (2015) Standard test method for flow of hydraulic cement mortar. ASTM International, West Conshohocken, PA.
[49] Wu X, Shen Y, Hu L (2022) Performance of geopolymer concrete activated by sodium silicate and silica fume activator. Case Stud Constr Mater 17:e01513. https://doi.org/10.1016/j.cscm.2022.e01513
[50] Cornelis R, Priyosulityo H, Satyarno I, Rustendi I (2022) Effect of the mortar volume ratio on the mechanical behavior of class CI fly ash-based geopolymer concrete. Civil Eng J 8(9):1920–1935. https://doi.org/10.28991/CEJ-2022-08-09-012
[51] Alanazi H, Yang M, Zhang D, Gao Z (2017) Early strength and durability of metakaolin-based geopolymer concrete. Mag Concr Res 69(1):46–54. https://doi.org/10.1680/jmacr.16.00118
[52] Al-Majidi MH, Lampropoulos A, Cundy A, Meikle S (2016) Development of geopolymer mortar under ambient temperature for in situ applications. Constr Build Mater 120:198–211. https://doi.org/10.1016/j.conbuildmat.2016.05.085
[53] ACI 318 (2019) Building code requirements for structural concrete and commentary. American Concrete Institute, Michigan, USA.
[54] Wahbi A, Pham DT, Hassen G, Garnier D, de Buhan P (2021) Experimental investigation on reinforced concrete beams subjected to axial compressive and shear forces. Struct Concr 22(6):3692–3710. https://doi.org/10.1002/suco.202100395
[55] Huang Z, Chen W, Hao H, Chen Z, Pham TM, Tran TT, Elchalakani M (2021) Shear behaviour of ambient cured geopolymer concrete beams reinforced with BFRP bars under static and impact loads. Eng Struct 231:111730. https://doi.org/10.1016/j.engstruct.2020.111730
[56] Escrig C, Gil L, Bernat-Maso E, Puigvert F (2015) Experimental and analytical study of reinforced concrete beams shear strengthened with different types of textile-reinforced mortar. Constr Build Mater 83:248–260. https://doi.org/10.1016/j.conbuildmat.2015.03.013
[57] Deepa Raj S, Ramachandran A (2019) Performance of hybrid fibre reinforced geopolymer concrete beams. SN Appl Sci 1(12):1725. https://doi.org/10.1007/s42452-019-1788-2
[58] Umniati BS, Risdanareni P (2017) Flexural test of fly ash based geopolymer concrete beams. In: Proceedings of the MATEC Web of Conferences. EDP Sciences, France. https://doi.org/10.1051/matecconf/20179701030
[59] Darmawan MS, Bayuaji R, Sugihardjo H, Husin NA, Anugraha Affandhie R B (2019) Shear strength of geopolymer concrete beams using high calcium content fly ash in a marine environment. Buildings 9(4):98. https://doi.org/10.3390/buildings9040098
[60] Sedan D, Pagnoux C, Smith A, Chotard T (2008) Mechanical properties of hemp fibre reinforced cement: Influence of the fibre/matrix interaction. J Eur Ceram Soc 28(1):183–192. https://doi.org/10.1016/j.jeurceramsoc.2007.05.019
[61] Awwad E, Mabsout M, Hamad B, Farran MT, Khatib H (2012) Studies on fiber-reinforced concrete using industrial hemp fibers. Constr Build Mater 35:710–717. https://doi.org/10.1016/j.conbuildmat.2012.04.119
[62] ASTM C1609 (2019) Standard test method for flexural performance of fiber-reinforced concrete (using beam with third-point loading). ASTM International, West Conshohocken, PA, USA.
[63] Huang Z, So CS, Chen W, Htet PM, Hao H (2024) Mechanical properties of basalt macro fibre reinforced geopolymer concrete. Constr Build Mater 438:136974. https://doi.org/10.1016/j.conbuildmat.2024.136974
[64] Eurocode 2 (2005) Design of concrete structures – Part 1–1: General rules and rules for buildings. CEN, Brussels.
[65] DM 204 (2022) Decreto Ministeriale n. 204 del 1.7.2022: Linee guida per la classificazione e gestione del rischio, la valutazione della sicurezza ed il monitoraggio dei ponti esistenti (in Italian).
[66] fib MC2020 (2023) Model code for concrete structures 2020. Fédération Internationale du Béton, Lausanne, Switzerland.
[67] SIA 262 (2012) Construction en béton (in French). Société Suisse des Ingénieurs et Architectes, Zürich, Switzerland.
[68] CSA A23.3-04 (2004) Design of concrete structures. Canadian Standards Association, Toronto, Canada.
[69] JSCE (2007) Standard specification for concrete structures. Japan Society of Civil Engineers.

[70] BS 8110-1 (1997) Structural use of concrete. British Standards Institution, London.
[71] AS 3600 (2018) Concrete structures. Standards Australia, Sydney.